NATIONAL AERONAUTICS AND SPACE ADMINISTRATION

Technical Report 32-1303

Solar Proton Forecast System and Procedures Used During the Mariner V Mission

Charles C. Gonzalez
Edward L. Divita

JET PROPULSION LABORATORY
CALIFORNIA INSTITUTE OF TECHNOLOGY
PASADENA, CALIFORNIA

October 1, 1968

NATIONAL AERONAUTICS AND SPACE ADMINISTRATION

Technical Report 32-1303

Solar Proton Forecast System and Procedures Used During the Mariner V Mission

Charles C. Gonzalez
Edward L. Divita

JET PROPULSION LABORATORY
CALIFORNIA INSTITUTE OF TECHNOLOGY
PASADENA, CALIFORNIA

October 1, 1968

TECHNICAL REPORT 32-1303

Prepared Under Contract No. NAS 7-100
National Aeronautics & Space Administration

Preface

The work described in this report was performed by the Project Engineering Division of the Jet Propulsion Laboratory.

Acknowledgment

The authors wish to thank Robert Doeker and the personnel in the Space Disturbance Forecast Center, Environmental Sciences Service Administration, Boulder, Colorado, for valuable suggestions and assistance in the development of the forecast procedures described herein and for providing preflare forecasts and preflare and flare-associated data. The authors also wish to thank Don Robbins and his associates in the Radiation and Fields Branch at the Manned Spacecraft Center, Houston, Texas, for valuable suggestions in the use of solar radio emission data as a real-time predictor of solar proton event time-integrated flux and for providing real-time access to radio emission data from the Solar Particle Alert Network Observatories. Thanks are also due Arthur Covington, Radio and Electrical Engineering Division of the National Research Council, Ottawa, Canada, for providing 2800-MHz solar radio burst profiles. Finally, this work was made possible by the Mariner 67 Project, through Dan Schneiderman and Conway Snyder.

Contents

Contents (contd)

Tables

Contents (contd)

Tables (contd)

Figures

Contents (contd)

Figures (contd)

Abstract

A solar forecasting system and forecasting procedures for predicting the time of occurrence of solar proton events and the associated time-integrated proton flux on a real-time basis for the *Mariner V* mission are discussed. The solar forecasting system utilizes solar activity data obtained from solar observational networks and provided by the Space Disturbance Forecast Center (SDFC) at Boulder, Colorado. Since SDFC does not provide forecasts of proton events and their sizes on a real-time basis, statistical methods are developed, based on past solar cycle data, in order to use the solar activity data obtained on a real-time basis in predicting proton events and their sizes. The 2800-MHz radio burst energy is correlated with time-integrated proton flux. Several other solar parameters are correlated with time-integrated proton flux. However, none results in a better correlation. In addition, procedures for receiving data, making forecasts, and reporting the forecasts to the project on a real-time basis are described. Statistical uncertainties in the prediction method and uncertainties in the data are discussed, and their influence on the value of the predictions is evaluated. A brief history of the real-time forecasting of proton events using the method and procedures is presented. This history indicates that the forecast system and the forecast procedures have both scientific and engineering applications during the operational phase of a long-term interplanetary mission. Finally, recommendations are made to improve forecasting techniques and forecast procedures for reliable and timely warnings of pending solar proton events and their sizes.

Solar Proton Forecast System and Procedures Used During the *Mariner V* Mission

I. Introduction

The *Mariner V* mission to Venus took place during the time period June–October 1967, when moderate to large proton events were expected, based on statistical analysis of past solar cycle data. Radiation tests of selected spacecraft subsystems demonstrated that exposure to proton fluxes as large as those expected during the *Mariner V* mission could significantly degrade the performance of critical spacecraft subsystems. Consequently, real-time forecasting of proton events and their sizes during the operational phase of the mission was desired so that the spacecraft operation team could, if necessary, implement options to use subsystems insensitive to proton radiation. In addition, if proton events were forecast during the mission, mission operations could be altered to allow collection of fields and particle data. Therefore, the *Mariner V* Project Office supported the development of a real-time forecast system.

Only short-term real-time predictions of solar flare proton events and their sizes are expected to provide an adequate forecast during an interplanetary mission because of the gross uncertainties associated with long-term predictions.

Methods of forecasting solar proton events and procedures for using the forecasts during the *Mariner V* mission on a real-time basis were developed utilizing data from the solar observational network made available through the Space Disturbance Forecast Center (SDFC) in Boulder, Colorado. SDFC also provides short-term prediction of solar activity, which can be used to establish periods of probable solar proton activity but does not currently predict proton event sizes. In addition, the Manned Spacecraft Center (MSC) is developing the Solar Particle Alert Network (SPAN) to predict the proton radiation to which astronauts may be exposed during the Apollo mission. SPAN is combined with solar observatories operated by SDFC and the Air Weather Service of the USAF to form the National Solar Flare Patrol. The methods and forecasting system presented here utilized the radio and solar observatories of the National Solar Flare Patrol as data sources for making real-time forecasts.

The forecast methods are based on statistical analyses of solar activity data and solar proton flux from the past solar cycle. In the statistical analyses several parameters of solar activity coincident with the occurrences of solar flares were correlated with the time-integrated proton flux which usually follows the large solar flares. The best correlations were obtained through single-parameter correlations of the 2800-MHz radio burst energy as the predictor of proton event time-integrated flux. However, the peak 2800-MHz radio flux will be used as a preliminary predictor to provide early alert since the peak radio flux may occur after as little as 20% of the radio burst is completed.

The forecast methods were incorporated into a forecast system and operational procedures were established for reporting forecasts to the *Mariner V* Project. The sun, however, was unexpectedly inactive during the course of the *Mariner V* mission.

In addition, statistical analyses were performed on past cycle data to estimate the average time available after a forecast for operational considerations and the reliability of the forecast methods. The results indicate that there is sufficient time after the occurrence of a solar flare and radio event to forecast an expected large proton event before the arrival of a significant amount of radiation near earth and within the trajectory of *Mariner V*. The results also demonstrate that forecasts of events at or above the threshold level established for Venus of 2×10^{10} protons/cm^2, for energy > 30 MeV, have an estimated false alarm probability between 0–40%.

When the threshold radiation levels are exceeded, the forecasts have both scientific and engineering applications; when the thresholds are not exceeded, the predictions have only scientific applications. Forecast procedures are established to account for both of these applications. The procedures presented cover generally a time span from 28 days before a solar flare or radio event until after an observed proton event is completed or an expected proton event is considered a false alarm.

II. Requirements for Solar Forecast System and Procedures

The requirements for a solar proton event forecasting system and procedures for using forecasts during the *Mariner V* mission are divided into two parts: engineering requirements and scientific requirements. Engineering requirements are related to possible radiation effects on spacecraft subsystems; scientific requirements are related to data which may be obtained when a solar proton event occurs.

A. Engineering Requirements

The engineering requirements for a solar proton event forecasting system are that the predictions be reliable and that adequate warning time be provided prior to the occurrence of proton events larger than established radiation flux criteria.

The established proton radiation flux criterion for reporting forecasts to the Project based on predictions made near earth is that the time-integrated proton flux must be 10^9 protons/cm^2 or greater having energy greater than 30 MeV within the 95% confidence band. This criterion is based on the radiation test threshold levels listed in Table 1, which were established for radiation-sensitive *Mariner IV* subsystems and components (Ref. 1). The criterion was derived from the level of 2×10^{10} protons/cm^2 having energy greater than 33 MeV, which is the level at which the more sensitive subsystems were tested and no significant degradation was observed. Because the predictions are made near earth and the worst condition for spacecraft exposure is at Venus encounter, it was necessary to reduce the level of 2×10^{10} protons/cm^2 at the spacecraft to a corresponding value of 1×10^{10} protons/cm^2 near earth to account for the assumed inverse square of the distance effect. Then this level was reduced to 1×10^9 protons/cm^2 to account for the uncertainties in the measured proton fluxes taken during the last solar cycle and the uncertainties in making a prediction based on near-earth data and extrapolating the data to near Venus. Consequently, when the prediction made near earth is 10^9 protons/cm^2 having energy greater than 30 MeV, the actual flux near Venus may be as much as 2×10^{10} protons/cm^2 having energy greater than 30 MeV.

The peak flux requirement was obtained from a regression equation for peak flux as a function of time-integrated flux rather than from the radiation test threshold damage level of 6.0×10^5 protons/cm^2-s having energy above 40 MeV (See Table 1). The comparable peak flux derived from the regression equation corresponding to the threshold time-integrated flux of 10^9 protons/cm^2 is 6.5×10^3 protons/cm^2-s ($E > 30$ MeV). As a result, the peak flux requirement is conservatively established for the spacecraft subsystems as 10^4 protons/cm^2-s having energies greater than 30 MeV because it is lower than the radiation test threshold level for peak flux. In addition, the predicted peak flux will be consistent with the predicted time-integrated flux from which it is obtained through the regression equation.

The amount of after-prediction time required to implement counter-measures before a significant flux is encountered was not established by the Project Office. However, limits on the time available based on the capabilities of the forecast method presented using data of the past solar cycle were taken from Section IV-C. The time limits are:

Table 1. Results of high-energy proton testing of *Mariner IV* subsystems and components[a]

Subsystem/ components	Test levels		Remarks
	Flux rate, protons/cm^2-s	Integrated flux, protons/cm^2	
Data encoder	8×10^6 to 1×10^7	4.3×10^{10}	No transient damage; no permanent damage
Squibs	3.9×10^7 ($E > 60$ MeV)	2.1×10^{10} ($E > 60$ MeV)	No significant degrading effects
Batteries		2×10^{10} ($E > 60$ MeV)	No apparent effect on spacecraft batteries at about 10^{10} protons/cm^2
Solar cells (Silicon P/N, 1Ω-cm)	1×10^7	2.1×10^{10} ($E > 36$ MeV)	No transient effects; loss of power, P/P_0 range 0.73–0.80
Command control and sequencing subassemblies	2.0×10^7	8.55×10^{10} to 1.02×10^{11}	No observable effects
Sun sensor	3.5×10^7	2×10^{10}	No observable effects
Canopus tracker	6×10^5 ($E > 40$ MeV)	2×10^{10}	Failed at listed flux-rate (loss of roll control)

[a] $E > 33$ MeV unless otherwise indicated.

(1) An average time delay of 0.7 h (using the lower 95% confidence limit on the average) between the time at which the RF emission ends and the start of the proton event, including the time for data transmission and making the prediction.

(2) An average time delay of 3.1 h (using the lower 95% confidence limit on the average) between the time at which the RF emission ends and the maximum of the proton event, including the time for data transmission and making the prediction.

These limits are expected to be conservative for an engineering application because they include small radio events and small proton events, both of which are usually associated with shorter periods.

Prediction reliability requirements were not established by the Project Office. However, estimates of the reliability available based on the capabilities of the forecast method presented using data of the past solar cycle were taken from the false alarm study results presented in Section IV-D. The estimated probability that the proton event will occur when the predicted time-integrated proton flux is 10^9 protons/cm^2 ($E > 30$ MeV) and greater is between 60 and 100%. This probability range for proton fluxes greater than 10^9 protons/cm^2 was determined based on the estimates of probability from the data samples in the flux range between 10^7–10^{10} protons/cm^2.

B. Scientific Requirements

For scientific applications of the forecasting system it is required that predictions be reliable and timely forecasts of the occurrence and size of proton events. Events of any size are of scientific interest, but predictions must be reliable enough to establish a tracking priority since tracking is usually being shared with other spacecraft and satellites. Again, the reliability requirement and the time required after the prediction to implement spacecraft tracking were not established. Results were based on the capabilities of the method presented and indicate the reliability and the time available for arranging tracking time.

III. General Considerations

A. Solar Activity

The level of solar activity is generally measured by the sunspot number computed over a specified period of time (Ref. 2). The sunspot number is obtained from $S_n = K(S + 10g)$, where S is the total number of sunspots, g is the total number of groups determined from a single observation by a specified observatory, and K is a weighting factor dependent on the characteristics of the observatory and determined in such a way that a uniform set of sunspot numbers is derived from different observatories (Ref. 2). Solar activity as indicated by the sunspot number exhibits a quasiperiodic behavior with a mean frequency of about 11 yr and with known limits on the observed cycles ranging from 7 to about 16 yr. The activity indicated by the sunspot number is usually averaged over consecutive months or years. Although the occurrence of a particular sunspot group does not mean that solar activity will follow, observations indicate that as the number of sunspots on the solar disk increases, the general solar activity increases. The regions near sunspots are normally sources of various types of solar activity which may result in the emission of particles and electromagnetic radiation.

Sunspot data from the past 215 years have been analyzed statistically to predict the level of solar activity expected in the current cycle and the time of maximum activity (Refs. 3 and 4). These predictions, using the average yearly sunspot number, give only the expected solar activity averaged over a period of 1 yr. The sun must be observed regularly to predict the occurrence of solar flares and the emission of particles. Active regions, called plages and faculae, whose temperature and brightness are higher than the surrounding areas are present on the sun. Sunspots are almost always found in plages. High magnetic fields are frequently found in regions near sunspots. Temperature gradients between cooler sunspots and hotter surrounding areas cause regions of stress which lead to transient solar activity such as solar flares. Forecasts of solar flare activity can be made as much as a month prior to an event, but for increased accuracy are made between 3 days and several hours prior to the event and are based on plage size and brightness, sunspot area and class, sunspot magnetic configuration, radio emission, past history of the active region, and other solar disk and limb features. When a flare occurs, there is an increase in solar electromagnetic emission in the optical, ultraviolet, X-ray, and radio frequency range. Protons have been measured from the same region in which radio emissions occur. However, not all radio emissions are associated with proton events, and conversely. Typical solar activity occurrences are shown in Table 2 as a function of time.

Table 2. Occurrence of solar activity on the sun and detection at earth as a function of time

Time	Occurrence of events on the sun	Detection of events at earth
−3–0 day	Growth of active regions	Optical observation of plages, sunspots, and magnetic complexity.
0	Beginning of solar flare	
0–10 min	Occurrence of solar flare with increased optical, X-ray, ultraviolet, and radio emissions (including 2800-MHz burst) followed by proton emission.	Direct detection of solar flare emissions and indirect detection by measurement of ionospheric effects. Commencement of arrival of 2800-MHz radio burst emission.
10 min–1 h		Recording of 2800-MHz radio burst emission
1–4 h		Arrival of protons
1–10 h		Characteristic rise of proton flux
10–20 h		Peak of moderate flux proton event (10^7–10^8 protons/cm^2)
20–40 h		Peak of high flux proton event ($>10^8$ protons/cm^2)
100–150 h		Termination of proton events

B. Solar Proton Events

The releases of energy which occur at the time of a solar flare occasionally include the emission of charged particles from the sun which reach the earth from 30 min to several hours later. These particles when defined as solar cosmic rays consist of protons having energies above 5–10 MeV and may extend to energies up to 20 BeV and more.

Predictions of average monthly and yearly proton fluxes using a predicted sunspot number and the past solar cycle proton flux have been made (Refs. 3 and 4). These prediction techniques were derived statistically, based on the correlation of past cycle proton data with sunspot number data. One study also involved the correlation of proton flux with average total sunspot area.[1] Predictions using these techniques may be made for periods of 6 months preceding the end of a solar cycle. Predictions of yearly proton fluxes are useful in planning a mission but do not give time of occurrence or size of an individual proton event; instead, they give an average expected proton flux for a specific time period in the future.

The data taken during the past solar cycle indicate that as the solar cycle approaches solar maximum and solar activity increases, flares and proton events become more numerous. Exceptionally large proton events of the last cycle occurred in a period of 2 to 3 years before and after the solar maximum. Solar maximum for the current solar cycle was predicted to occur during the 1968–69 time period; consequently, large proton events were expected during the *Mariner V* mission.

Based upon events of the past cycle, with few exceptions, the occurrence of a solar proton event can be associated with the occurrence of a flare. Moderate to large events ($\geqq 5 \times 10^7$ protons/cm^2 at $E > 30$ MeV) are usually preceded by a solar flare generally of class 2b or greater (see Appendix A for a discussion of flare classification). A prediction of occurrence of a flare of class 2b or greater along with other conditions such as a large, magnetically complex associated sunspot group indicates the possibility of the occurrence of a pending solar proton event. However, some of the electromagnetic radiation occurring at the time of a flare may be associated directly with proton emission. Furthermore, electromagnetic radiation will propagate through space much faster than solar particles and may reach the earth several hours before the arrival of solar particles (see Table 2). Thus it may be possible to use this radiation to predict the occurrence and size of a solar proton event. The energy radiated in

[1]Private communication from S. Pierce, JPL.

the 2800-MHz solar radio burst coincident with the occurrence of the flare may be considered a predictor of proton events.

IV. Predicting Solar Proton Events and Sizes Using Solar Radio Emission

A. Theoretical Considerations

Radio emission from the sun covers a broad range of frequencies and types of emission. Various types of emission are produced, e.g., thermal radiation, synchrotron radiation, and bremsstrahlung. However, the only type that has been consistently related to solar proton events is the type IV continuous broad-band emission caused by synchrotron radiation. This emission is divided into various component types as shown in Fig. 1 (from Ref. 5). The RF emission of interest is the centimeter wavelength radio burst in the region of 3 to 30 cm (microwave) with main emphasis on the 10.7-cm (2800-MHz) bursts. This emission as shown in Fig. 1 is included in the type IV μ region. A sample burst is shown in Fig. 2 (from Ref. 6). A centimeter outburst, sometimes referred to as a microwave outburst has a peak intensity which usually is greater than 100 flux units.[2] These bursts usually last more than 10 min and up to approximately 1 h or more.

The outbursts at microwave frequencies are believed to be synchrotron emission caused by electrons (0.5 to 5 MeV) constrained temporarily by magnetic fields in the solar chromosphere and corona. It is generally assumed that the flare mechanism which accelerates electrons to relativistic energies also accelerates protons and heavier nucleons to subrelativistic and relativistic energies. The high-energy nucleons escape directly from the solar plasma (Ref. 8). The lower energy nucleons are part of the plasma which eventually leaves the sun. The mean energy of accelerated electrons seems to be nearly independent of the intensities of the outburst. Therefore, the intensity of the outburst is not a measure of the energy of the accelerated electrons, but rather a measure of the number of accelerated electrons (Ref. 9). If we assume that an equal number of positive ions and electrons are accelerated and that the majority of positive ions accelerated are protons, then it follows that the total energy radiated should be directly related to the time-integrated proton flux. Therefore, the correlation of type IV solar radio emission with solar proton events may be simply a case of correlating phenomena which are physically related.

[2]One flux unit = 10^{-22} W/m^2-Hz (Ref. 7).

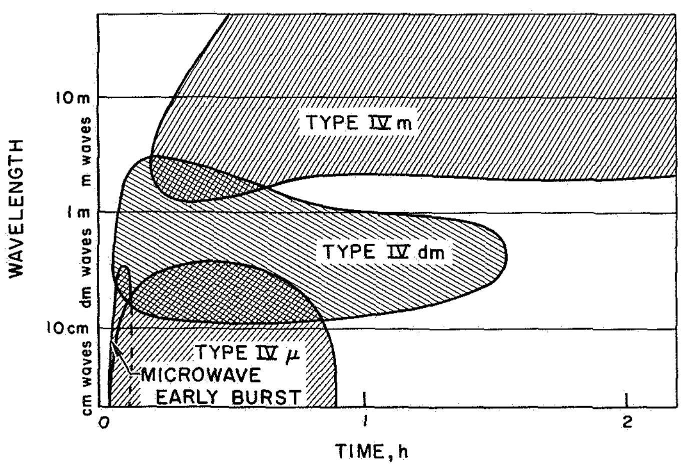

Fig. 1. Model of the composite spectra of solar type IV radio emission in the range 10,000 to 25 MHz

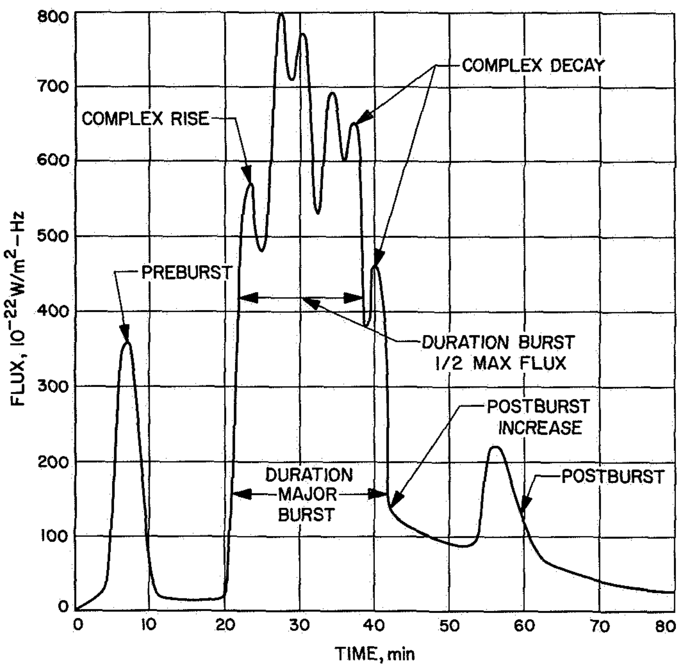

Fig. 2. Model of a fixed-frequency (centimeter wavelength) outburst associated with a solar proton event (from Ref. 6)

B. Solar Data from the Last Solar Cycle

Radio burst data were compiled to obtain a source of selected radio burst parameters.[3,4] A compilation is presented in Table 3 along with various other solar activity

[3]Private communication from M. D. Lopez, Manned Spacecraft Center, Houston, Tex.

[4]Private communication from A. Covington, Canadian National Research Council, Ottawa, Canada.

Table 3. Optical and radio parameters of solar activity used in correlation, false alarm, and miss frequency analyses of RF data and proton events

Date	Plage area[a]	Plage brightness	Sunspot area[a]	Flare importance[b]	Flare location		RF peak intensity, 10^{-22} W/m²-Hz	RF burst energy, 10^{-18} J/m²-Hz	Time-integrated flux for $E>30$ MeV, protons/cm²	RF burst, UT		Burst duration, min	Particle rise time, h	Particle onset time, UT
					Lat	Long				Start	Max			
6/18/55	6,000	4.0	639	3	S22	W21	1575	43		1907	1908			
7/9/55			No flare data available				309	30		1906	1922			
2/16/56	8000[c]	4.0	1734–1437	2	N20	E08	650	60		1757	1813			
2/19/56	18,000[c]	3.5	1734–1437	1+	N25	W23	650	29		1427	1435			
3/13/56	10,000	3.5	1237	2	N21	E50	850	14		1452	1454			
3/15/56	9000[c]	3.0	1089	2	N22	E21	1300	43		1622	1627			
6/20/56			No flare data available				340	12		1938	1939			
8/31/56					N16	E16	>340 off scale	>61	2.5×10^7	1231				1430
9/17/56	17,500[c]	3.5	361	2+	S20	W17	320	13		1940	1947			
11/13/56	4000	3.5	814–465	2	N16	W10	180	13	1×10^8	1433[d]	1440			2000
12/26/56	3000	3.5	1002	2	S17	W11	915	132		1403	1454			
1/6/57	5000	3.5	2089–1351	1–	N16	W53	585	42		1758	1827			
4/12/57	5100	3.0	369–237	2	S25	W73	525	12		1855	1900			
4/14/57	6000	3.5	937–665	1	S23	W28	37	40		1700	1915			
4/16/57	9000	3.0	1000–432	3	N30	E85	1650	87		1043	1050			
4/17/57	9000	3.0	1000–432	3+	N20	E69	6000	546		2006	2042			
6/3/57	4500	3.0	787	3	S18	W18	290	17		1042	1051			
6/19/57	9000	3.5	931	2	N20	E45	2325	34	No estimate	1608	1610			
7/15/57			No associable flare				300	12		2019	2043			
7/16/57	1200	2.5	769–530	1+	S33	W28	350	23		1741	1756			
7/20/57			No associable flare				145	14		1735	1750			
7/24/57	5500	3.0	504	3	S24	W27	1100	94	7.5×10^6	1759[d]	1838			2015
8/1/57	6500	3.5	1092–845	1	S35	E04	25	22		1400	1815			
8/9/57	6200	3.5	1092–845	1	S33	W77	40	27	1.5×10^6	1304[d]	1517			1600
8/28/57	8200	3.0	774	2+	S28	E30	760	10	No estimate	2017	2019			0000(8/29)
8/31/57	8000	3.5	1317	3	N25	W02	3900	350	8.0×10^7	1300[d]	1321	65.0		1500
9/2/57	6000	3.5	626	2+	S34	W36	120	30	5.0×10^7	1300[d]	1324			1700
9/3/57	15,000	3.5	597	3	N23	W30	1350	51		1417	1426			
9/18/57	6800[c]	4.5	1998	3+	N20	E02	275	47		1821	1825			
9/21/57	5500	4.0	491	3	N10	W06	790	13	1.5×10^6	1330[d]	1337	14.5		1700
9/26/57	19,500	3.0	232	3	N22	E15	110	25	4.0×10^5	1915[d]	1945	60.0		2100
10/20/57	14,200	3.5	2373	3+	S26	W35	4000	209	5.0×10^7	1640[d]	1651	51.0		2100
11/4/57		No burst recorded				No logical flare association			9.0×10^6	No burst				0200
1/15/58	9000	3.5	786	2+	S13	W58	1350	21		1640	1643			
6/5/58	4000	3.0	314	2+	S18	E69	387	35		1614	1623			
6/28/58	12,000	3.0	245–114	1–	S26	W20	23	32		1500	1745			
7/30/58	19,000[c]	3.0	1795–901	2	S13	W64	400	15		1525	1529			
8/2/58	19,000[c]	3.0	1795–901	1–	S14	W90	2050	26		1840	1842			
8/22/58	6400	3.5	1192	3	N18	W10	1500	192	7.0×10^7	1430[d]	1506	120	10.0	1530
10/24/58	7000	3.5	439	2+	S05	W57	185	18		1439	1511			
12/11/58	8500	3.0	1318–710	2	S02	E00	1225	14		1805	1810			
12/12/58	10,000	3.5	1318	2+	S03	W08	1500	20		1257	1301			
1/21/59	7500	3.5	1886–1476	3	N10	E48	600	12		1702	1708			

Table 3 (contd)

Date	Plage area[a]	Plage brightness	Sunspot area[a]	Flare importance[b]	Flare location Lat	Flare location Long	RF peak intensity, 10^{-22} W/m^2-Hz	RF burst energy, 10^{-18} J/m^2-Hz	Time-integrated flux for $E > 30$ MeV, protons/cm^2	RF burst, UT Start	RF burst, UT Max	Burst duration, min	Particle rise time, h	Particle onset time, UT
1/24/59	2400	3.5		1	S06	E20	60	12		1450	1535			
	6000	3.0		1	N18	W21								
1/25/59	13,000[c]	3.0	1400–945	2	N18	W50	325	50		1410	1412			
2/9/59	4000	3.0	1064–866	2+	N09	E87	160	10		1308	1317			
3/22/59	8500	4.0	2274–1732	1+	N29	W50	525	12		1340	1345			
4/17/59	4000	3.5	513–264	2	N10	E84	51	26		1350	1450			
5/8/59	11,000	3.5	806–5563 1152–947	2+	N21	E83	2220	29		2254	2257			
5/10/59	19,000	3.5	1552–947	3+	N18	E47	2550	811	9.6×10^8	2100[d]	2154		20.0	0030(5/11)
5/11/59	17,500	3.5	806–563 1152–947	3	N10	E41	900	75		2010	2021			
6/9/59	9000	3.5	1111–856	2	N17	E90	1800	146		1645	1740			
6/18/59	9000	3.5	1111–856	3+	N16	W12	1225	14		1139	1140			
7/9/59	12,000	3.5	1981–1412	2	N18	E67	520	15		2043	2046			
7/9/59	12,000	3.5	1981–1412	2	N19	E48	520	30		2112	2128			
7/16/59	12,000	3.5	1981–1412	3+	N16	W31	5500	732	9.1×10^8	2118[d]	2154		12.0	0000(7/17)
8/31/59	7500	3.0	1011–536	1+	N10	E11	270	10		1858	1906			
12/2/59	9000	3.5	2622–1948	2+	N07	W16	875	11		1246	1248			
12/4/59	13,000	3.0	2622–1948	2+	N06	W44	40	16		1815	1910			
1/11/60	3500	2.5	575	3	N22	E03	220	13	4.0×10^5	2056[d]	2108		6	0300(1/12)
1/15/60	5000	3.5	1150	2	S20	W68	700	117	No estimate	1340	1357			0300(1/16)
3/28/60	3000	3.5	1650	2	N14	E37	1150	127		2048	2118			
3/30/60	3500	3.0	1650	2	N12	E11	1750	160	6.0×10^6	1518[d]	1556			0300(3/31)
4/3/60	No associable flare						75	18		1745	2122			
5/4/60	4500	2.5	850	3	N13	W90	600	69	6.0×10^6	<1025	1046		2–3	1030
5/6/60	3900	4.0	<500	3+	S09	E07	695	69	4.0×10^6	1406[d]	1434	90	3.0	1800
6/25/60	2500	3.5		3	N21	E06	425	46	No estimate	1148	1209			1700
7/27/60	2500	3.5		3	N22	W27	140	17	No estimate	2140	2158			~2300
8/11/60	13,000	3.5	1100	2+	N22	E26	1100	26	6.0×10^5	1923	1928			~0000
9/16/60	3500	4.0	925	1	S22	E67	2000	185		1702	1756			
10/23/60	3500	3.0	1225	1+	N22	E90	320	22		2056	2122			
11/6/60	5800	3.0		3	N13	E07	56	20		1628	1837			
11/12/60	8000	4.0	1775	3+	N27	W04	5500	606	2.4×10^9	1320[d]	1346	40	10.0	1400
11/20/60	Flare and radio burst associated with proton event uncertain				N25	W90	400	25	4.5×10^7	2023	2027			
12/5/60	7500	3.5		3+	N26	E74	330	23	No estimate	1828	1838			~0500(12/6)
7/11/61	4000	4.0	1400	3	S07	E32	1500	138	3.0×10^6	1604[d]	1745		8–10	0000(7/12)
7/12/61	5700[c]	3.5	1400	3	S07	E23	1200	88	4.0×10^7	<1102	1113		8–12	1300
7/15/61	5700[c]	3.5	1400	2	S07	W20	111	36	1.3×10^7	1510[d]	1610			1545
7/20/61	5600	3.5	1400	3	S06	W90	1800	94	5.0×10^6	1552[d]	1621	42	4–6	0300(7/21)
9/10/61	6000	3.5	1350	1	N08	W80	900	95	4.0×10^7	1930[d]	2001		10.0	2100
9/28/61	3600	3.0	<500	3	N13	E29	800	36	6.0×10^6	2211[d]	2218		1.5	2330
11/10/61	2200	3.0		1+	N19	W90		8	8×10^6					

[a]Plage and sunspot area, solar disk $\times 10^{-6}$.
[b]Because of conversion difficulties, current notation is not used.
[c]Complex grouping of plage regions; area given is for plage region associated with event.
[d]Events used in calculation of RF burst duration and delay times from radio events to proton events.

parameters and proton event data (Refs. 6, 10, and 11). The time-integrated proton flux for the 9/26/57 event was estimated from statistical analyses connecting the time-integrated proton flux above 30 MeV with that above 100 MeV. Some of the RF burst energies presented in Table 3 for the 2800-MHz radio emissions have been previously correlated with solar proton event time-integrated flux.[3] Previous studies were also performed to correlate peak radio flux, duration of the burst, and average radio flux with proton flux. In addition, 3750-MHz data have been considered. The results of these studies indicate that correlations made with the 2800-MHz radio emission and the time-integrated proton flux are more significant than those obtained using the 3750-MHz radio emission. This does not rule out the possibility that further study of the 3750-MHz data might also provide good correlation when new data are available.[3] However, the correlations described in this report use only 2800-MHz data, except for those presented in Section IV-D-3. Further correlation studies might include the frequency of approximately 2695 MHz since this is the frequency being used by the MSC observatories which will provide the radio data for use in SPAN (Ref. 12). When new data are taken at various frequencies and when past cycle data are refined, new frequencies or a combination of frequencies may be used to demonstrate more significant correlations.

Table 4. Estimates of the duration of 2800-MHz bursts associated with proton events of the last cycle and of delay time between bursts and proton events

Duration time, min	60.3 ± 29.1
Delay time between start of RF to start of proton event, h	3.9 ± 1.4
Delay time between start of RF to maximum of proton event, h	8.6 ± 3.7
Delay time between maximum of RF to start of proton event, h	3.3 ± 1.4

A statistical analysis was performed to obtain the average radio burst duration and the delay times between bursts and proton events for those events given in Table 3 for which data were available. These are the same solar events which were used in making the correlations between 2800-MHz burst data and time-integrated proton flux. Table 4 lists the average and the estimated 95% confidence limits on the average for the delay time from maximum and start of radio burst to the start of the proton event and from the start of the radio burst to the maximum of the proton event and the time of burst duration. Figure 3 (from Ref. 13) shows an envelope and mean of the time history of solar proton events of the past solar cycle and the time history of three different solar proton events.

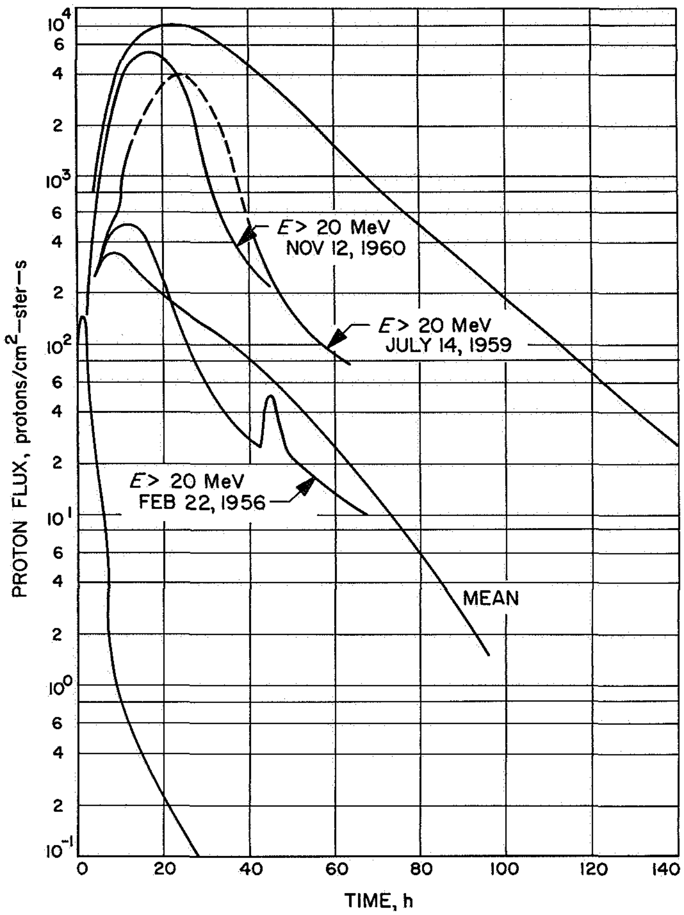

Fig. 3. Time history envelope and mean of the flux of proton events compared with three events of the last solar cycle (from Ref. 13)

C. Correlation of Radio Emission Parameters with Time-Integrated Proton Flux

The data used in the analyses of 2800-MHz radio bursts are given in Table 3 and consist of 81 radio events and 24 associated proton events.[5] The solar events for which only radio events are listed may have been associated with proton events that were undetected because the fluxes were below earth-based detector cutoffs or did not arrive at the earth because of propagation conditions or trapping in space. The results presented, using the radio events and the RF predictions techniques, were based on all 81 radio events.

1. Single-parameter correlations. Correlations were made between the $\log_{10}$ of the 2800-MHz radio burst

[5] Also M. D. Lopez (see footnote 3).

energy and the $\log_{10}$ of the associated time-integrated proton flux having energies greater than 30 MeV. The correlations were made using a total of 24 radio events observed by the Canadian National Research Council Observatory at 2800 MHz. A linear least squares analysis was performed using the data, and the correlation coefficient and regression equation were found. The linear regression analysis was performed with the listed 24 data points (See Table 3) and the 13 points selected as described below.

The regression analysis was performed first with data from the 24 events and then with data from 13 events selected from the 24. The selection of the 13 points was made by statistically analyzing the data to discard outliers (See Fig. 4). This was accomplished by computing the average proton flux and the standard error of the mean for a particular interval of radio energy. Those events whose proton flux was greater than 3 times the standard error of the mean (3S) were eliminated. The procedure was repeated with the remaining points in the interval. If no events were eliminated on the first or successive trials, then all events whose proton flux was greater than 2S were eliminated and the procedure repeated until no events were eliminated. After this was done, 16 points remained. At this point, a check was made to see if the differences of the averages of neighboring intervals exceeded $3S_D = 3(S_{x1}^2 + S_{x2}^2)^{1/2}$, where S_{x1} is the standard error of the mean of interval 1 and S_{x2} the standard error of the mean of interval 2. The differences of the averages did exceed $3S_D$ for three intervals which had radio energies greater than 40 flux units (50–100, 100–500, 500–1000) representing moderate to large radio and proton events. Thus, a linearly increasing relationship between the log of RF energy and the log of proton fluxes truly exists only at the upper ranges of the curve of radio energy vs proton flux. Because of the large scatter of data, the events with radio energy less than 40 radio energy flux units were neglected, it being assumed that major interest is centered on the large events. A linear least squares analysis was performed and the correlation coefficient was calculated for the remaining 13 points. The correlation coefficient is 0.962; thus a linear regression approximation was considered applicable. The linearity of the relationship between radio energy and proton flux for the large events was used over the entire range of radio events in all of the analyses of this section (again because major interest is centered on the large events). However, the results of the analyses for radio events of less than 40 radio energy flux units are questionable. The solid line in Fig. 4 indicates the region over which use of a linear relationship is justified on the basis of the tests described above; the dashed line indicates the region over which it is not.

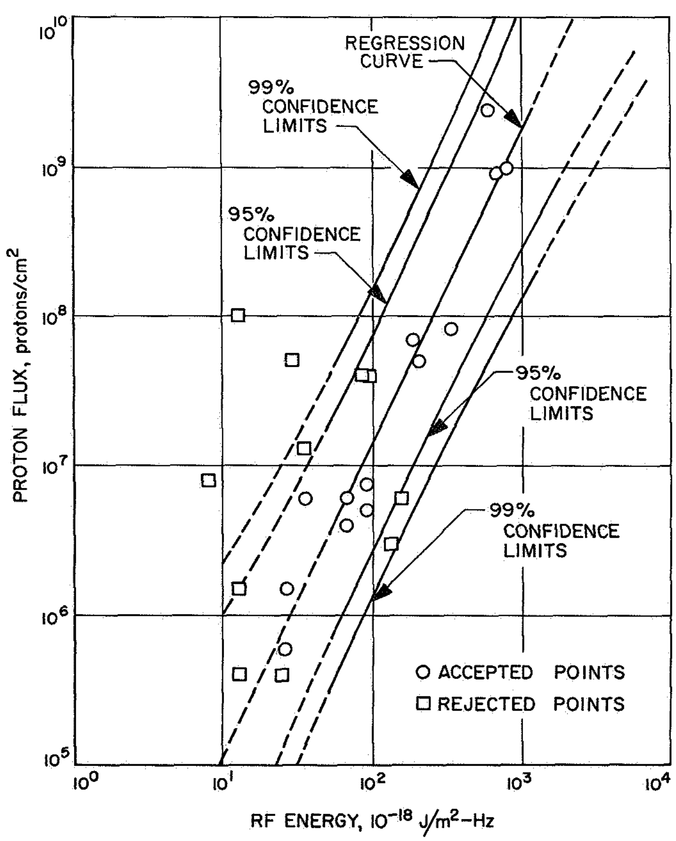

Fig. 4. Time-integrated proton flux having energy greater than 30 MeV as a function of RF burst energy

Equations (1) and (1a) give the regression equations for the selected 13 data points and the total 24 data points, respectively. See Table 3 for the values used:

$$\log_{10}(PF) = 2.976 + 2.083 \log_{10}(RFE) \qquad (1)$$

$$\log_{10}(PF) = 4.778 + 1.285 \log_{10}(RFE) \qquad (1a)$$

where

PF = is the time-integrated proton flux for energies greater than 30 MeV (protons/cm²)

RFE = radio burst energy in units of (10^{-18} J/m²-Hz)

The correlation coefficients with the 95% confidence intervals are 0.962 (0.873, 0.989) and 0.716, (0.432, 0.871) for the 13 and 24 points, respectively. Figure 4 shows the relationship between radio burst energy and proton event flux derived from Eq. (1) which is used to predict time-integrated proton flux having energy greater than 30 MeV from the area of the associated RF burst profile at 2800 MHz.

The 95% and 99% confidence intervals for the prediction of a single-event time-integrated proton flux were determined for Eq. (1). The prediction of a single-event time-integrated proton flux will lie in the following confidence interval (Ref. 14):

$$Y' \pm t_{\alpha/2} S_{yx} \left(1 + \frac{1}{n} + \frac{(X - \bar{X})^2}{(n-1) S_x^2}\right)^{1/2} \tag{2}$$

where

$t_{\alpha/2}$ = the percentage point of the student t-distribution

$1 - \alpha$ = confidence interval

X = $\log_{10}$ of radio energies at which confidence limits were computed

$\bar{X}$ = $\log_{10}$ of average radio energy

$$S_{yx} = \left(\sum_{i=1}^{n} \frac{(Y_i - Y_i')^2}{(n-2)}\right)^{1/2} \tag{3}$$

= estimated standard deviation of predicted flux of proton event from actual flux of proton event

$$S_x = \left(\sum_{i=1}^{n} \frac{(X_i - \bar{X})^2}{(n-1)}\right)^{1/2} \tag{4}$$

= estimated standard deviation of radio burst energy of actual events from the average event energy

Y_i = $\log_{10}$ of observed proton flux of the selected events

Y_i' = $\log_{10}$ of predicted estimate of integrated proton flux from regression equation

X_i = $\log_{10}$ of the radio energies of the selected events.

For the 95 and 99% confidence intervals, $S_{yx} = 0.317$, $S_x^2 = 0.279$, $t_{0.025} = 2.201$, and $t_{0.005} = 3.106$.

Several things must be taken into account when using these confidence limits. First, the confidence limits and regression equation must be applied with caution below 40 radio energy flux units. Secondly, the confidence limits were determined based on the S_{yx} computed for all data points instead of an S_{yx} computed for each interval of data points, which effectively cancelled the resolution available for the grouping of the data. However, this effect is assumed to be negligible, except for the smaller events near and below 40 flux units. Finally, the 95 and 99% confidence limits apply only when a proton event follows a radio event because these limits were determined based on the correlation between radio event energies and associated time-integrated proton fluxes. The probability that a proton event will occur is presented below.

For each of the 81 radio burst energies the predicted value of proton flux from Eq. (1) and the 95% confidence interval was compared with the actual value of proton flux associated with that event. If the actual value fell within the 95% confidence interval, it was counted as a successful prediction. If the actual value fell below the 95% confidence interval, or if no proton event occurred after detection of a radio event, the event was called a "false alarm." The occurrence of a proton event of smaller magnitude than predicted is important in engineering applications. In this application there are threshold limits established for radiation damage to the spacecraft from solar proton events. A prediction of an event of size greater than these limits which is followed by an event of size less than these limits would have to be considered

Table 5. False alarm percentage and miss frequency for the prediction method using RF energy and the 95% confidence limits on time-integrated proton flux estimates

Time-integrated proton flux, protons/cm^2	Number of predicted events	Number of false alarms	False alarms, %	Number of misses
$(1–10) \times 10^5$	39	31	79.5	0
$(1–10) \times 10^6$	23	17	74	2[c]
$(1–10) \times 10^7$	14	8	43[a] 14.3[b]	3
$(1–10) \times 10^8$	4	1	25	1
$(1–10) \times 10^9$	1	0	0	0

[a]No proton event occurred.
[b]Proton event occurred.
[c]No burst recorded in one case.

Table 6. False alarm percentage and miss frequency for the prediction method using RF energy and the 99% confidence limits on time-integrated proton flux estimates

Time-integrated proton flux, protons/cm^2	Number of predicted events	Number of false alarms	False alarms, %	Number of misses
$(1–10) \times 10^5$	39	31	79.5	0
$(1–10) \times 10^6$	23	17	74	2[a]
$(1–10) \times 10^7$	14	6	43	2
$(1–10) \times 10^8$	4	1	25	1
$(1–10) \times 10^9$	1	0	0	0

[a]No burst recorded in one case.

a false alarm even though an event of some magnitude did occur. However, from the standpoint of scientific applications an event of any size is significant.

False alarm analyses were performed in two ways. Using the first method, the RF energy range was divided into intervals corresponding to predictions of proton flux in the ranges 1 to 10×10^n (protons/cm^2), where $n = 5$ through 9 consecutively. The criterion for selecting a false alarm was then applied.

Because of the scarcity of data from the last solar cycle, especially at the higher flux ranges, the false alarm probability is questionable. The information available, however, is given in Tables 5 and 6 and Fig. 5. There was no significant change in the false alarm percentage in going from a 95% confidence interval to a 99% confidence interval. Of all the false alarms given in Tables 5 and 6, only two events resulted from the case of a radio burst which

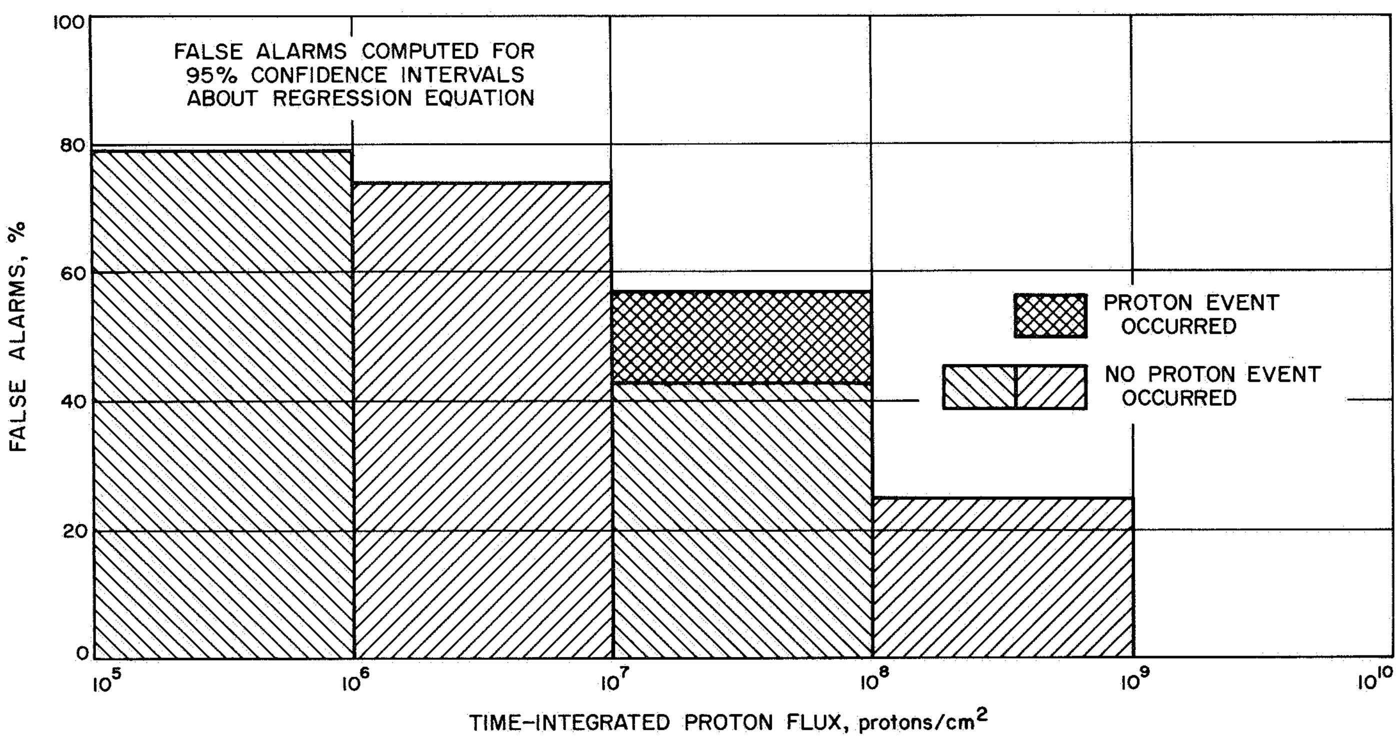

Fig. 5. False alarm percentage for RF energy and time-integrated flux ($E > 30$ MeV) prediction method

gave a prediction of a higher flux than the actual flux; these false alarms did not result when the 99% confidence intervals were used. These two events resulted in predicted fluxes (including their 95% confidence intervals) that were higher than the actual flux by a factor of about 1.2 and 1.7, respectively. Factors of 1 to 2 or less cannot be considered very significant because of uncertainties in the value of the proton flux. The rest of the false alarms resulted from radio bursts in which no proton event was detected.

In the above analysis, the event was called a miss if the actual value fell above the upper 95% confidence limit or if a proton event occurred during the time interval when the 2800-MHz radio flux was being observed and no RF was detected. The possibility of a flux being higher than predicted might not be important in scientific applications, but it is extremely important in engineering applications.

Although Tables 5 and 6 give a number of misses, only one miss occurred where no radio burst was recorded (11/4/57 proton event). The others resulted from time-integrated proton flux predictions whose estimates plus the 95% confidence interval were less than the actual proton flux. Four of the misses involved a flux higher than the 99 or 95% intervals by the following factors: one by about a factor of 4 and 8 (8×10^6 protons/cm^2 actual flux), two by about a factor of 5 and 10 (4.5×10^7 to 5×10^7 protons/cm^2 actual flux), and one by a factor of 33 and 60 (1×10^8 protons/cm^2 actual flux). Except for the latter miss, these misses were not considered significant because they occurred for low proton flux events. Another miss involved a prediction higher than the 95% confidence interval by a factor of only 1.45, which is less than the uncertainty error in the measured proton data. The number of misses decreased by 1 when the 99% confidence interval about the estimate was considered.

Figure 6 and Tables 7 and 8 show the results of the second method of obtaining false alarm percentages and misses. In this analysis, a value of RF energy from Fig. 4 was chosen which corresponds to a specified proton flux value. The number of predicted events was compared with the number of false alarms for all predicted values above the flux value. Instead of taking a confidence interval about the predicted flux value, any value of proton flux which fell below the predicted level was counted as a false alarm. The false alarm percentages were obtained in one case by using the value of radio energy giving a particular estimate of proton flux (see Table 7) and in the other case by using the values of radio energy giving the

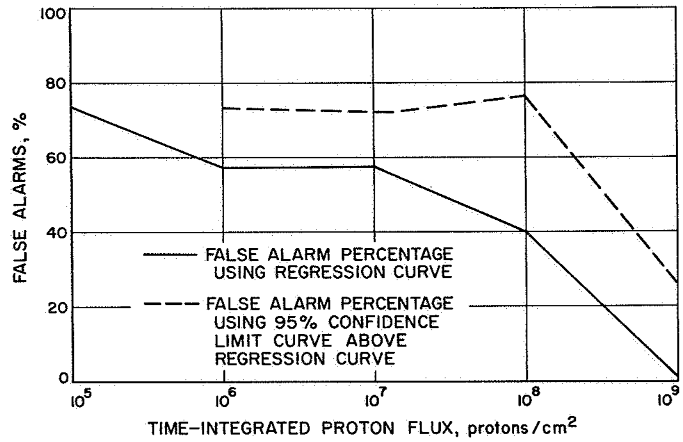

Fig. 6. Cumulative false alarm percentage for RF energy and time-integrated flux ($E > 30$ MeV) prediction method

same proton flux on the estimate plus 95% confidence limit curve (see Table 8). As shown in Fig. 4, the radio energy giving a particular flux decreases when the curves lying above the actual regression curve are considered. The reason for using the curve lying above the regression

Table 7. Cumulative false alarm percentage and miss frequency for the RF energy prediction method using the time-integrated proton flux estimates

Time-integrated proton flux, protons/cm^2	Number of predicted events	Number of false alarms	False alarms, %	Number of misses
$>10^5$	81	59	73	1
$>10^6$	42	24	57	5[a]
$>10^7$	19	11	58	5
$>10^8$	5	2	40	1
$>10^9$	1	0	0	1

[a]No burst recorded in one case.

Table 8. Cumulative false alarm percentage and miss frequency for the RF energy prediction method using the 95% confidence limits on time-integrated proton flux estimates

Time-integrated proton flux, protons/cm^2	Number of predicted events	Number of false alarms	False alarms, %	Number of misses
$>10^6$	81	59	73	1[a]
$>10^7$	32	23	72	3
$>10^8$	13	10	77	1
$>10^9$	4	1	25	0

[a]No burst recorded.

curve is that a lower miss frequency occurs at the lower radio energies. However, an increase in false alarms will occur if this is done. In this analysis, either of the two curves was chosen, and all events predicted above a certain flux were considered. For example, the number of events predicted above 10^9 protons/cm^2 would be the same as the number of radio events whose energy was equal to or greater than the energy on the curve which would give a value of 10^9 protons/cm^2. This was compared to the actual number of events which occurred with proton fluxes equal to or greater than 10^9 protons/cm^2, and the excess number of events over that number predicted would be the number of false alarms. A miss would be any event not preceded by a radio event or preceded by one less than the radio energy corresponding to that flux or greater.

The second method is useful in predicting false alarm probability for any estimate equal to or greater than a certain proton flux. Two curves were considered in the second method in order to analyze the tradeoff between the miss frequency and false alarm rate as the value of radio flux, used as a threshold for a particular proton flux or greater, was decreased. As can be seen from Tables 7 and 8, the false alarm percentage increased when the 95% confidence limit curve was used and the miss frequency decreased.

The false alarm probability and miss frequency selected for use with the radio burst energy predictor are obtained from the results in Table 5. When an estimate of the time-integrated proton flux within the 95% confidence limits is made, the probability of having a false alarm or miss is assumed to be the percentage of false alarms or misses presented in Table 5 except for those predicted events having time-integrated flux greater than 10^8 protons/cm^2. For these events the false alarm probability is given as a range. For those predicted events between 10^8–10^9 protons/cm^2 the false alarm probability is in the range of 25–40%, and for those between 10^9–10^{10} protons/cm^2 the false alarm probability is in the range of 0–40%. These false alarm probability ranges are based on the average false alarm probability for events in the interval 10^7–10^9 protons/cm^2 and the estimated false alarm probabilities for the intervals 10^8–10^9 and 10^9–10^{10} protons/cm^2. This rough approximation was made because the data sample in these last two intervals is considered inadequate to obtain representative false alarm probabilities for each interval.

Another parameter of the radio burst profile is the peak radio flux. The peak in the radio burst profile occurs early in the event, in most cases at least before the halfway point in time. Of 24 radio events, 23 were used in the correlation of the $\log_{10}$ of proton flux and the $\log_{10}$ of radio burst peak flux (one event had no recorded peak flux). The correlation coefficient (based on a linear least squares approximation) is 0.542. Data selection similar to that used in obtaining the regression of proton flux on radio energy was not used because the peak flux data were scattered in such a way as to make results of such an analysis difficult to interpret. However, events with peak radio fluxes less than 250 flux units were discarded because of the large amount of scatter for low peak fluxes. The second linear least squares analysis was made on the remaining 17 events. The regression curves are shown in Fig. 7 along with the 95 and 99% confidence limits on the predicted proton flux.

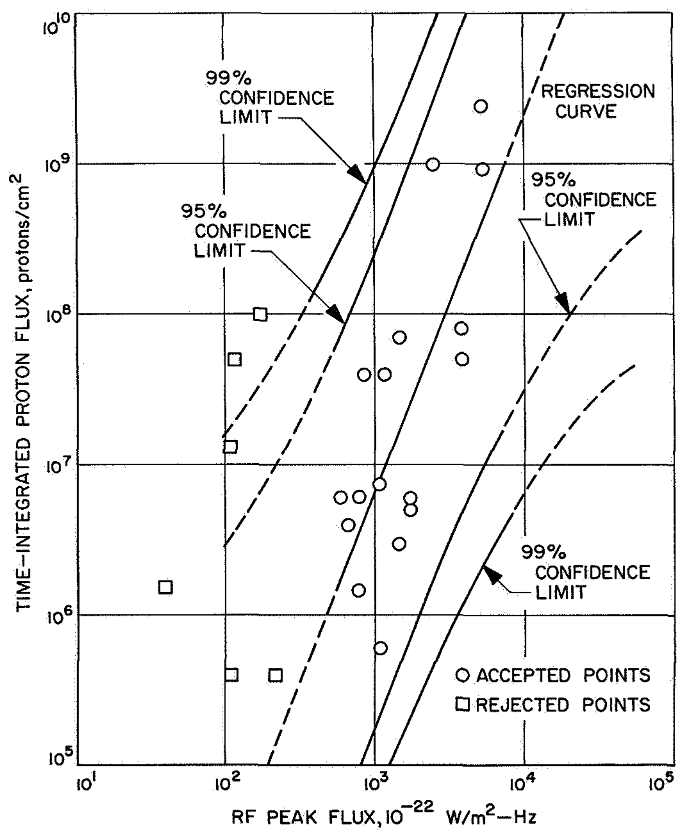

Fig. 7. Time-integrated proton flux for energies greater than 30 MeV as a function of RF burst peak flux

The linear regression equations found using the 17 and 23 events are given below in Eqs. (5) and (5a):

$$\log_{10}(PF) = 2.489 \log_{10}(peak) - 0.622 \qquad (5)$$

$$\log_{10}(PF) = 4.380 + 0.964 \log_{10}(peak) \qquad (5a)$$

where

$PF =$ the time-integrated proton flux for energies greater than 30 MeV (protons/cm^2)

and

$peak =$ the peak radio flux of the radio burst profile in units of 10^{-22} W/m^2-Hz

The correlation coefficients and 95% confidence limits on the correlation coefficients for the 17 and 23 event samples are 0.756 and (0.423, 0.909), and 0.542 and (0.158, 0.783), respectively.

Confidence limits of 95 and 99% were computed for the peak flux regression equation in the same manner as that for the radio energy. The standard deviation of predicted proton flux from the actual proton flux is $S_{yx} = 0.698$ for the $\log_{10}$ of the fluxes (see Eq. 3). The dotted lines (shown in Fig. 7) are used where the curve is extrapolated out of the range of data, and its use in these ranges is questionable.

The correlation of peak radio flux with proton flux is not as good as the correlation of radio energy with proton flux. In addition to the poorer correlation obtained using peak radio flux, it is difficult in some cases to define the peak flux with the same precision as the radio energy. The difficulty of determining the peak flux is demonstrated in Fig. 8 for a multiple peak radio event.

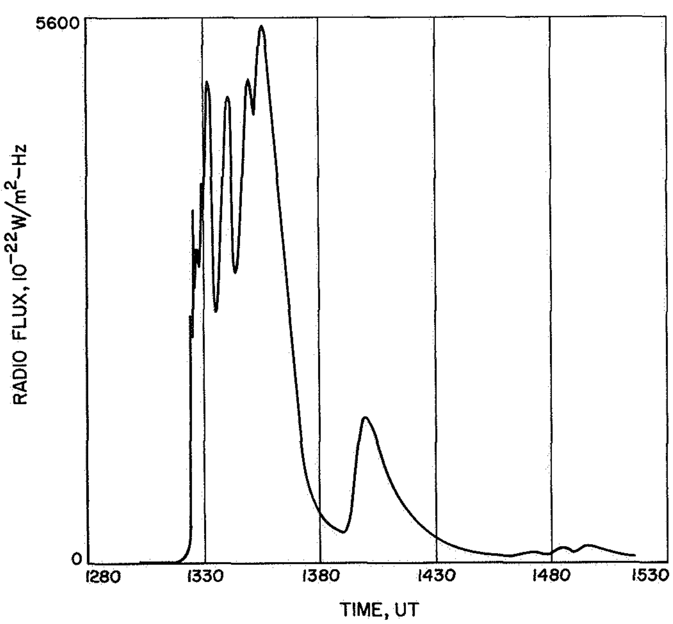

Fig. 8. Reconstruction, 2800-MHz radio burst profile of November 12, 1960

Table 9. False alarm percentage and miss frequency for the prediction method using RF peak flux and the 95% confidence limits on time-integrated proton flux estimates

Time-integrated proton flux, protons/cm^2	Number of predicted events	Number of false alarms	False alarms, %	Number of misses
$(1-10) \times 10^5$	34	26	76.5	0
$(1-10) \times 10^6$	22	15	68	1[a]
$(1-10) \times 10^7$	19	13	68.5	4
$(1-10) \times 10^8$	5	1	20	1
$(1-10) \times 10^9$	0	0	0	0

[a]No burst recorded.

Table 10. Cumulative false alarm percentage and miss frequency for the prediction method using RF peak flux and the time-integrated proton flux estimates

Time-integrated proton flux, protons/cm^2	Number of predicted events	Number of false alarms	False alarms, %	Number of misses
$>10^5$	80	57	71.2	0
$>10^6$	46	30	65.2	6[a]
$>10^7$	24	17	71	5
$>10^8$	5	3	60	2
$>10^9$	0	0	0	1

[a]No burst recorded in one case.

Table 11. Cumulative false alarm percentage and miss frequency for the prediction method using the RF peak flux and the 95% confidence limits on time-integrated proton flux estimates

Time-integrated proton flux, protons/cm^2	Number of predicted events	Number of false alarms	False alarms, %	Number of misses
$>10^6$	80	57	71.2	1[a]
$>10^7$	63	53	84.2	3
$>10^8$	37	34	92	1
$>10^9$	12	9	75	1

[a]No burst recorded.

The radio burst profile presented in Fig. 8 is that associated with the 11/12/60 proton event, one of the large proton events of the last solar cycle. The rate of change of radio flux in the burst in Fig. 8 at the leading edge of the burst profile is 978 flux units/min, and the highest flux

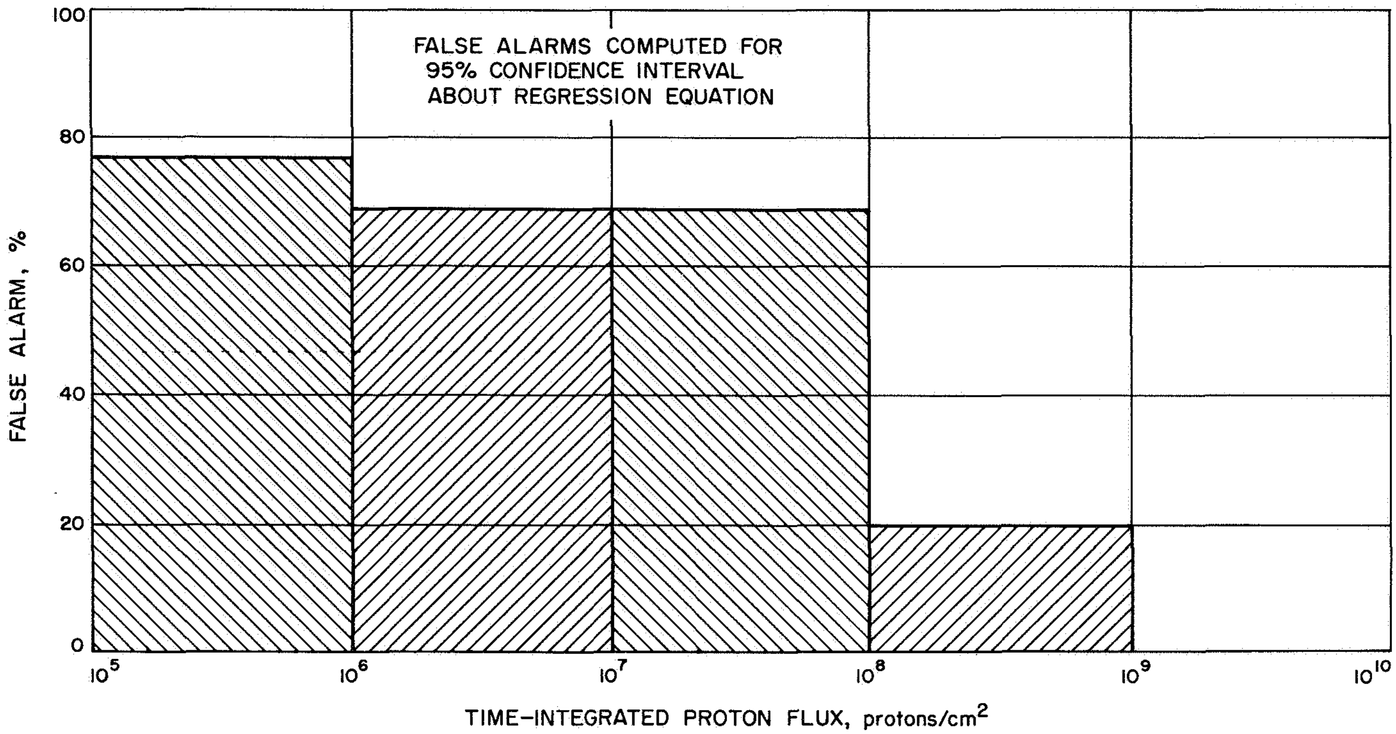

Fig. 9. False alarm percentage for RF peak flux and time-integrated flux ($E > 30$ MeV) prediction method

reached at the leading edge was about 5000 flux units. In Fig. 7 one can see that the peak radio flux giving an integrated proton flux of 10^9 protons/cm^2 (estimate plus 95% confidence interval) is about 1800 flux units. Therefore, after 2 to 4 min (plus time to obtain RF data) it would have been possible to predict a proton flux of 10^9 protons/cm^2 and be well inside the 95% confidence interval of the regression equation.

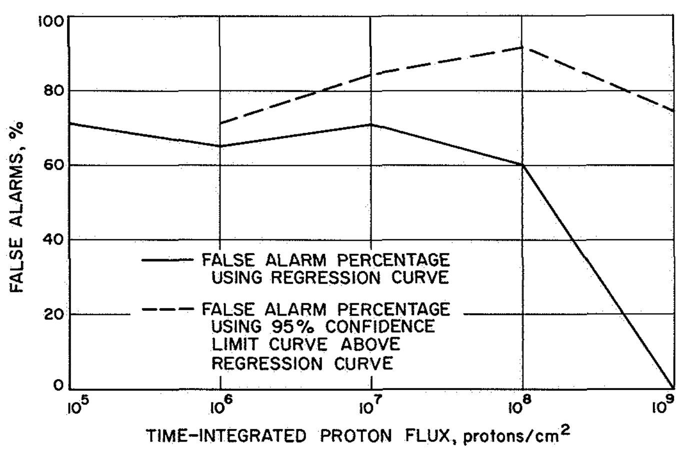

Fig. 10. Cumulative false alarm percentage for RF peak flux and time-integrated flux ($E > 30$ MeV) prediction method

A false alarm and miss frequency analysis similar to that described previously using the RF energy predictor was performed. The results are shown in Figs. 9 and 10, and Tables 9, 10, and 11. Again, most of the false alarms resulted from lack of occurrence of proton events. Many of the misses from the RF peak flux analysis were insignificant. The results of the false alarm and miss frequency analysis showed the same general characteristics as those discussed previously for the RF energy predictor.

The false alarm probability and miss frequency selected for use with the radio burst peak flux predictor is obtained from Table 9. The results of the false alarm probabilities are summarized below:

Time-integrated proton flux, protons/cm^2	False alarm probability, %
10^5–10^6	77
10^6–10^7	68
10^7–10^8	69
10^8–10^9	20–45
10^9–10^{10}	0–45

The above results were determined in the same manner as described previously for the RF energy predictor.

Table 12. Comparison of regression equations, correlation coefficients, and standard deviations derived in the linear least squares analysis of the solar activity parameters and proton event time-integrated flux

Description	1 parameter		3 parameters		5 parameters	
	13 events	24 events	13 events	23 events	13 events	23 events
Linear regression equations	$\log_{10}(PF) = 2.976 + 2.083 \log_{10}(RFE)$	$\log_{10}(PF) = 4.778 + 1.285 \log_{10}(RFE)$	$\log_{10}(PF) = 3.960 - 0.412 \log_{10}$ (plage area) $+ 0.161 \log_{10}$ (sunspot area) $+ 2.142 \log_{10}(RFE)$	$\log_{10}(PF) = 3.48 - 0.00507 \log_{10}$ (plage area) $+ 0.412 \log_{10}$ (sunspot area) $+ 1.309 \log_{10}(RFE)$	$\log_{10}(PF) = 4.326 - 0.445 \log_{10}$ (plage area) $+ 0.0602 \log_{10}$ (sunspot area) $+ 2.252 \log_{10}(RFE)$ $+ 0.0447 \log_{10}$ (plage brightness) $- 0.107 \log_{10}$ (flare importance)	$\log_{10}(PF) = 3.435 - 0.04874 \log_{10}$ (plage area) $+ 0.05785 \log_{10}$ (sunspot area) $+ 1.409 \log_{10}(RFE) +$ $0.4072 \log_{10}$ (plage brightness) $- 0.1133 \log_{10}$ (flare importance)
Linear correlation coefficients	0.962	0.716	0.964	0.750	0.965	0.767
Standard deviations	0.317		0.317		0.312	

2. *Multiple parameter correlation.* A multiple linear least squares analysis was used to find the correlation coefficient and the regression equation using five solar parameters as the independent variables and time-integrated proton flux as the dependent variable. These five solar parameters considered were the radio burst energy, the plage area, the plage brightness, the sunspot area, and the flare importance. The $\log s_{10}$ of the radio burst energy, plage area, sunspot area, and time-integrated proton flux were used. The analysis was performed for the 13 solar events used previously in the radio energy analysis and for 23 of the 24 events used previously (Table 3 and Figs. 11–14; there were incomplete data on one event).

A complete analysis on multiple parameters was not performed; rather only a simple analysis was made to compare regression equations and correlation coefficients obtained with the additional parameters with the ones obtained using only the radio energy. The quantity S_{yx} was computed for the equation using 13 events. The regression equations, correlation coefficients, and standard deviations S_{yx} obtained in the multiple parameter correlation analysis are given in Table 12, which compares all the regression equations and associated parameters.

The results given in Table 12 indicate that there are no major differences in the correlation coefficients and S_{yx}'s with use of the additional parameters. The regression equations show large fluctuation in the coefficients of the terms representing the parameters other than radio energy. Also, the coefficients of the terms for the other parameters are smaller than the coefficient of the radio energy term by at least a factor of 3. This means that time-integrated proton flux is better correlated with radio energy than with the other parameters.

3. *Other radio burst parameters.* The following radio burst parameters were correlated with the integrated proton flux for the associated proton event through a linear regression analysis (Figs. 15–17). The data in the frequency range 2800–3000 MHz were obtained at various observatories.

(1) Product of burst duration and peak flux. Burst duration alone was shown to have a poor correlation.[6]

(2) Time difference (min) between the maximum of the RF burst and flare maximum.

(3) Time delay (h) between the start of the proton event and the start of the RF burst.

Table 13 summarizes the correlation coefficients determined in this analysis.

Table 13. Summary of a correlation analysis of some radio burst parameters with integrated proton flux

Radio burst parameter	Correlation coefficient
1	0.607
2	(−) 0.260
3	0.060

These results indicate that only the correlation between the radio burst energy and the peak radio flux with the proton flux discussed previously is high enough to be useful.

[6]M. D. Lopez (see footnote 3).

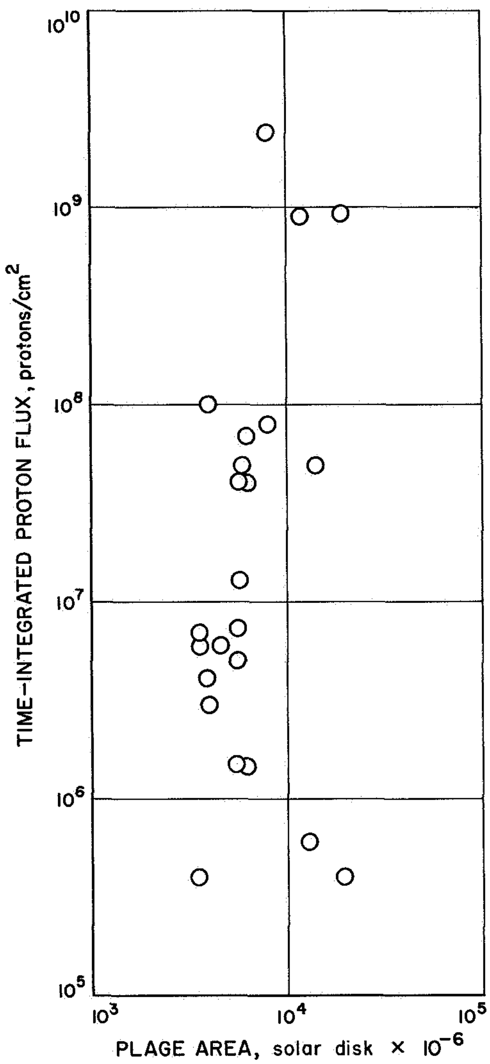

Fig. 11. Time-integrated proton flux having energy greater than 30 MeV as a function of plage area

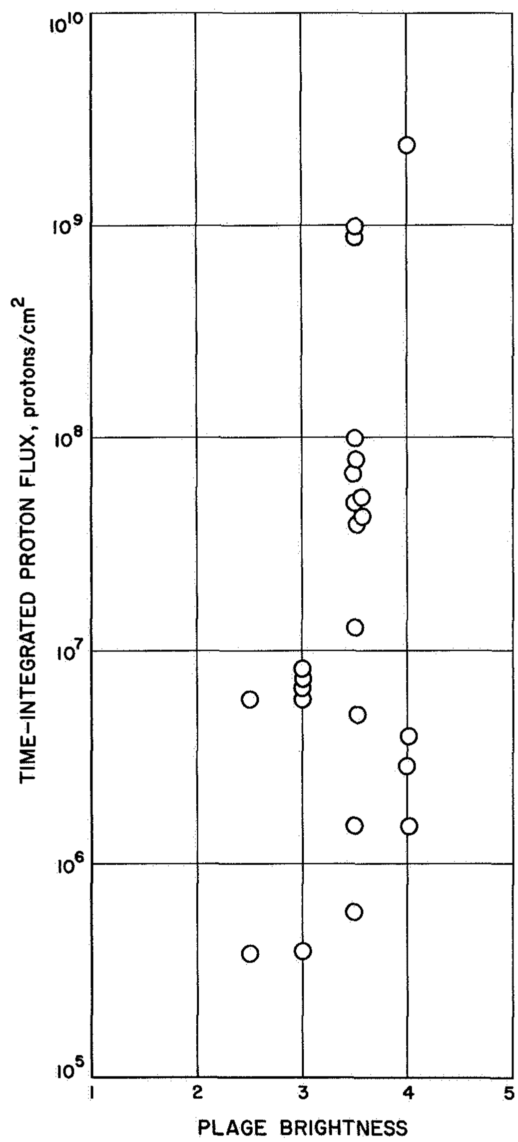

Fig. 12. Time-integrated proton flux having energy greater than 30 MeV as a function of plage brightness

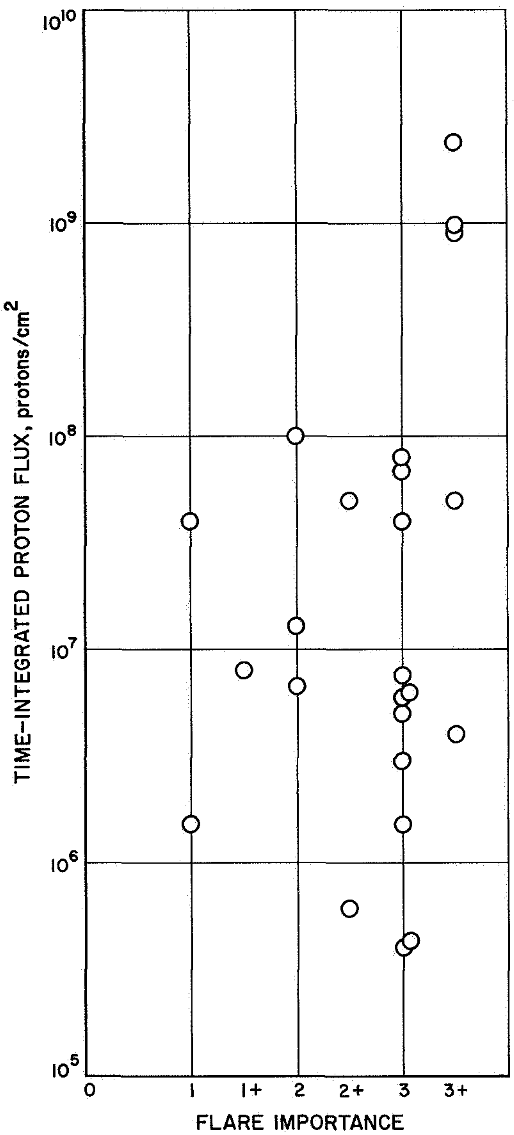

Fig. 13. Time-integrated proton flux having energy greater than 30 MeV as a function of flare importance (see Appendix A)

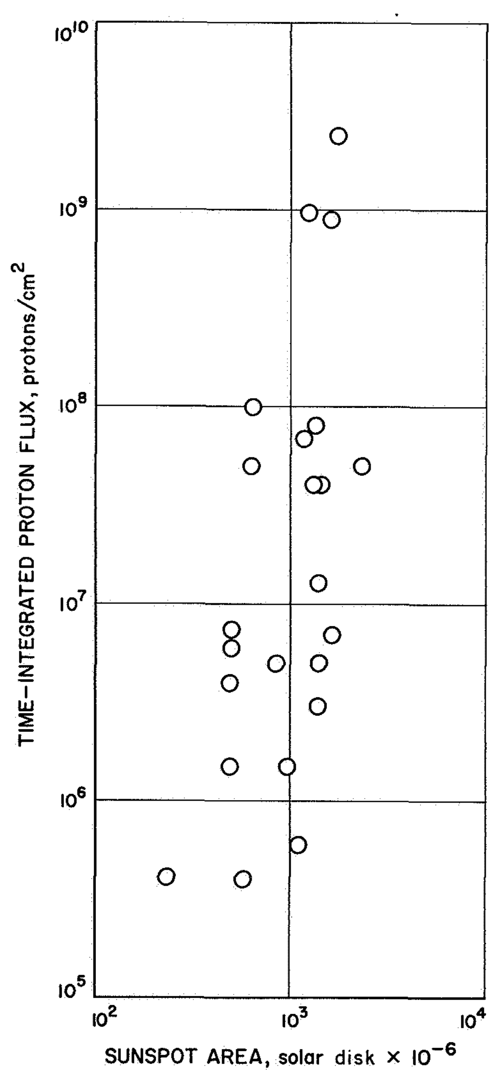

Fig. 14. Time-integrated proton flux having energy greater than 30 MeV as a function of sunspot area

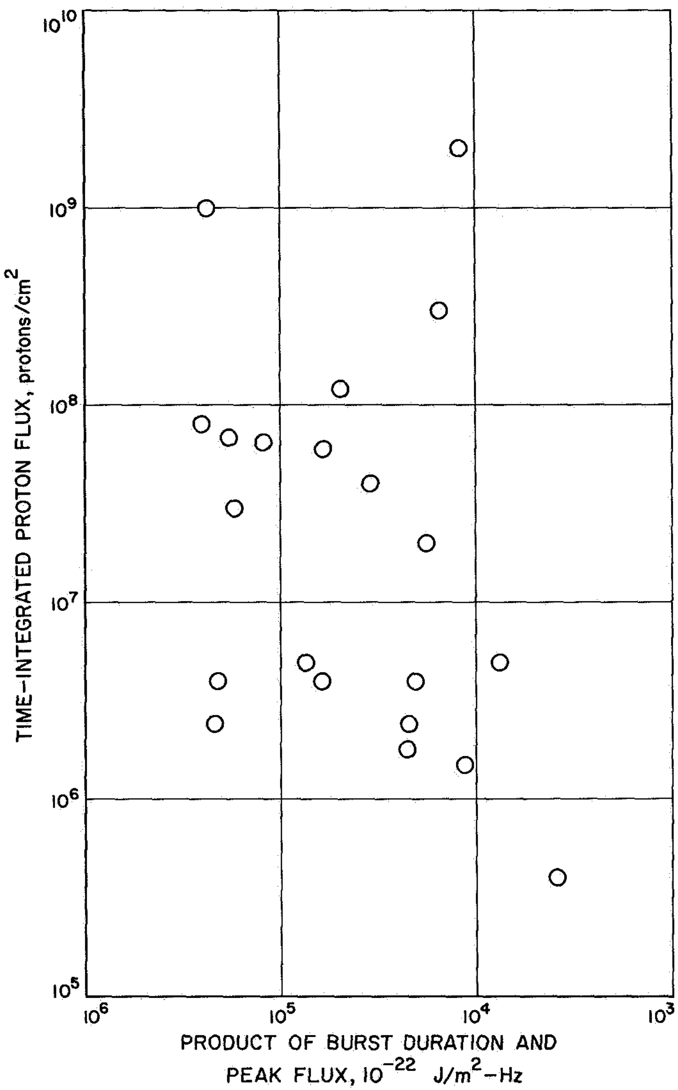

Fig. 15. Time-integrated proton flux having energy greater than 30 MeV as a function of the product of burst duration and peak radio flux

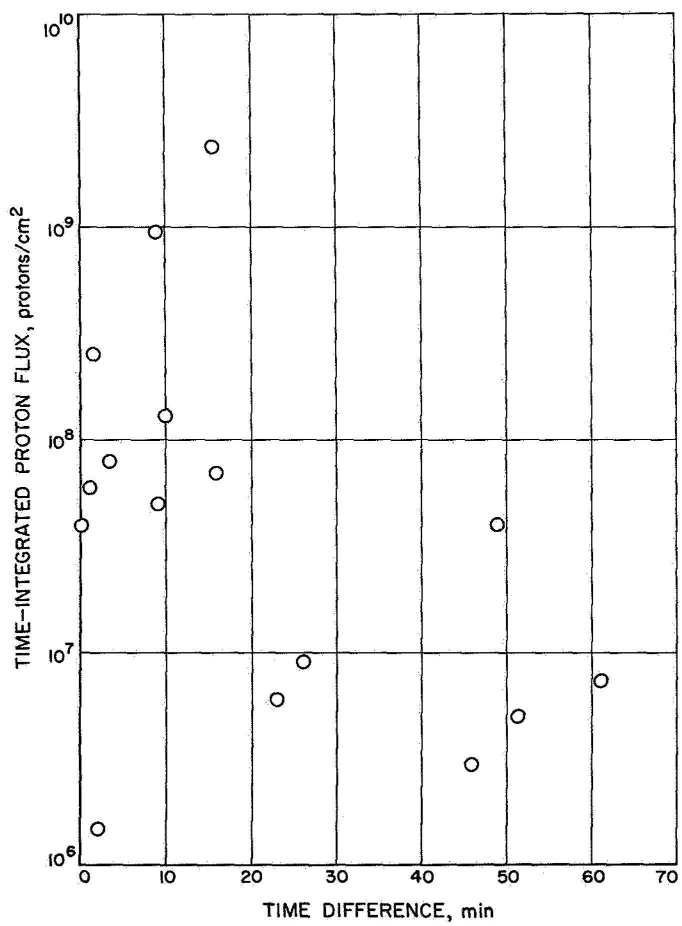

Fig. 16. Time-integrated proton flux having energy greater than 30 MeV as a function of the time difference between maximum of RF burst and flare maximum

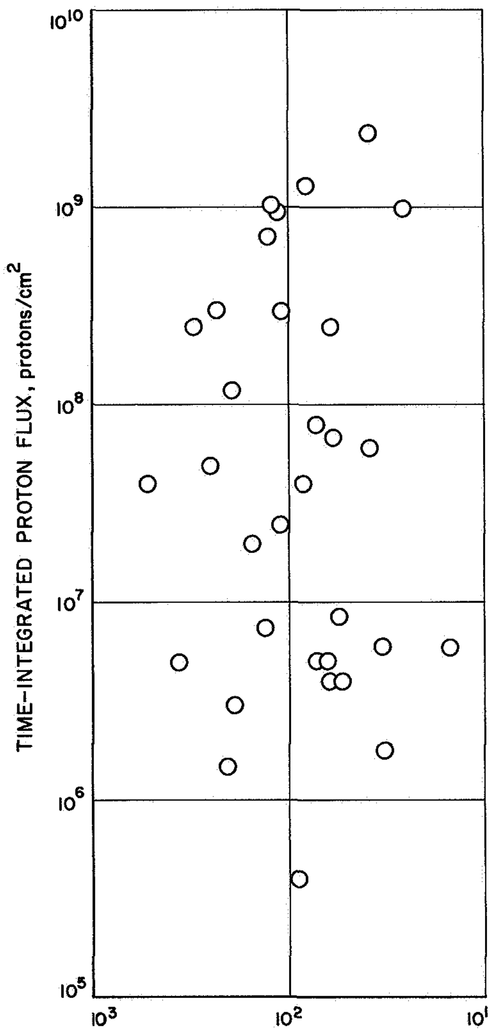

Fig. 17. Time-integrated proton flux having energy greater than 30 MeV as a function of the time delay between start of PCA and start of RF burst

D. Selection of Parameters and Techniques to Predict Proton Events

The regression equation relating time-integrated proton flux and radio burst energy (Eq. 1) is selected for making the final forecast of time-integrated proton flux on a real-time basis during long-term interplanetary missions. The regression equation relating time-integrated proton flux and peak radio flux (Eq. 5) is selected for making preliminary predictions of time-integrated proton flux when the observable peak radio flux indicates that a large event is expected. Equation (1) was selected on the basis of the value of its correlation coefficient. Equation (5) was selected on the basis of the timeliness of the forecast when using peak radio flux. False alarm percentages as a function of time-integrated proton flux (Tables 5 and 9) and estimated burst duration time and delay times given in Table 4 are selected for use in completing the evaluation of the forecasts.

A forecast of the associated peak proton flux of the pending proton event is obtained from Fig. 18, using the predicted time-integrated proton flux. The relationship between peak and time-integrated proton flux presented in Fig. 18 was determined by linear regression analysis, using data of the last solar cycle (Refs. 6 and 11 were used except as noted previously).

Confidence limits of 95% are also shown on Fig. 18 so that when the time-integrated proton flux is estimated, the peak proton flux with its associated 95% confidence limits may be estimated and compared with the threshold radiation levels established as requirements for alerting project personnel.

A summary of major parameters obtained by using the selected techniques is presented in Tables 14 and 15 for various values of radio burst energy and peak radio flux, respectively.

E. Limitations on Near-Earth Predictions Using Radio Emissions

Several limitations are inherently present when applying RF emissions observed near earth to techniques for forecasting proton flux in space. Propagation characteristics of solar protons in interplanetary space are such that the protons may reach certain points in interplanetary space without prior warning from a solar radio burst. This may be caused by proton events originating on the side of the sun away from the earth. In addition, the reception of radio energy at earth does not mean that all points in interplanetary space will contain solar protons. The particle propagation characteristics of the interplanetary medium will influence the arrival time of protons and determine whether or not they will arrive at all. This phenomenon is dependent on the position of the particle-producing flare on the sun's disk. Although the influence of the position of the flare on the arrival or nonarrival of protons at earth has been studied, no direct relationship has been found. Finally, the time for protons to travel from the sun to a spacecraft traveling to Venus may be considerably less than the time it takes them to arrive at earth. This would allow a shorter warning time than that based on observations from earth.

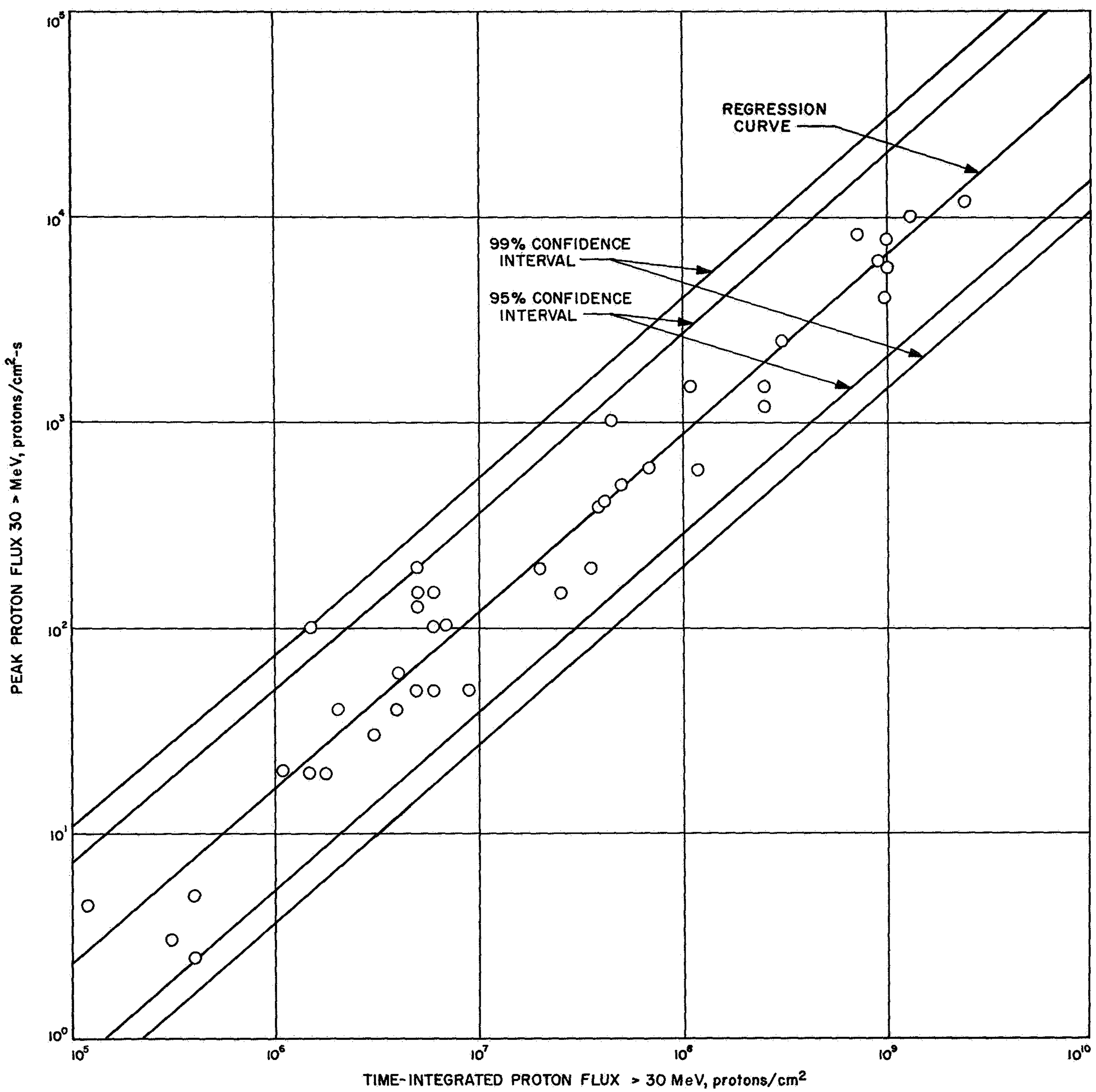

Fig. 18. Peak proton flux ($E > 30$ MeV) as a function of time-integrated proton flux ($E > 30$ MeV)

Table 14. Summary of statistical results of prediction of proton event fluxes on real-time basis using radio burst energy

Radio energy received on real-time basis, 10^{-18} J/m^2-Hz	Predicted proton time-integrated flux ($E > 30$ MeV) includes 95% confidence level, protons/cm^2		Probability of false alarm, %	Estimated range of time available after prediction, h		Estimated peak proton flux range ($E > 30$ MeV), protons/cm^2-s	Threshold level for proton time-integrated flux exceeded in the 95% confidence interval	Threshold level for proton peak flux exceeded in the 95% confidence interval
	Estimate	95% confidence interval		To start of proton event	To peak of proton event			
40	2.1×10^6	4.0×10^5–1.2×10^7	74	0.7–4.5	3.1–11.5	7.5×10^0–1.4×10^2	No	No
100	1.4×10^7	2.7×10^6–7.2×10^7	57	0.7–4.5	3.1–11.5	4.0×10^1–6.8×10^2	No	No
200	6.0×10^7	1.1×10^7–3.2×10^8	57	0.7–4.5	3.1–11.5	1.3×10^2–2.4×10^3	No	No
400	2.5×10^8	4.5×10^7–1.4×10^9	25–40	0.7–4.5	3.1–11.5	4.5×10^2–8.8×10^3	Yes	Yes
1000	1.7×10^9	2.7×10^8–1.2×10^{10}	0–40	0.7–4.5	3.1–11.5	2.1×10^3–5.8×10^4	Yes	Yes
2000	7.0×10^9	1.0×10^9–5.0×10^{10}	0–40	0.7–4.5	3.1–11.5	6.5×10^3–2.0×10^5	Yes	Yes

Table 15. Summary of statistical results of prediction of proton event fluxes on real-time basis using peak radio flux

Peak radio flux received on real-time basis, 10^{-22} W/m^2-Hz	Predicted proton time-integrated flux ($E > 30$ MeV) includes 95% confidence level, protons/cm^2		Probability of false alarm, %	Estimated range of time available after prediction, h		Estimated peak proton flux range ($E > 30$ MeV), protons/cm^2-s	Threshold level for proton time-integrated flux exceeded in the 95% confidence interval	Threshold level for proton peak flux exceeded in the 95% confidence interval
	Estimate	95% confidence interval		To start of proton event	To peak of proton event			
600	1.8×10^6	4.6×10^4–7.0×10^7	68	1.6–4.4	4–11.4	1.0×10^0–6.5×10^2	No	No
1000	6.5×10^6	1.8×10^5–2.2×10^8	68	1.6–4.4	4–11.4	3.9×10^0–1.8×10^3	No	No
3000	9.5×10^7	2.6×10^6–3.8×10^9	68	1.6–4.4	4–11.4	3.8×10^1–2.1×10^4	Yes	Yes
6000	5.5×10^8	1.2×10^7–2.5×10^{10}	20–68	1.6–4.4	4–11.4	1.3×10^2–1.0×10^5	Yes	Yes
10,000	1.9×10^9	3.0×10^7–1.2×10^{11}	0–45	1.6–4.4	4–11.4	3.1×10^2–4.3×10^6	Yes	Yes
30,000	3.0×10^{10}	1.6×10^8–5.6×10^{12}	0–45	1.6–4.4	4–11.4	1.3×10^3–1.4×10^7	Yes	Yes

V. Forecast Procedures for Predicting Proton Events

A. Data and Preflare Forecast Network

The network established to transmit solar data and information into centralized agencies consists of solar observatories located throughout the world. Two agencies have been established to provide forecasts of solar activity and solar proton events from preflare solar data: the Space Disturbance Forecast Center, in Boulder, Colorado, which provides forecasts and solar information to civilian agencies, and the Astrogeophysical Forecast Facility at Ent Air Force Base, Colorado, which provides forecasts and other information to military agencies. Figure 19 and Table 16 present information on the location of the observatories, observing hours, times at which data are reported, and methods of communication with SDFC.[7] The solar observatories use optical and radio telescopes to measure various solar parameters. SDFC obtains the data from the observatories to make forecasts and to fulfill special data requests made by its users.

[7]Private communication from R. Doeker, SDFC, Boulder, Colo.

The Manned Spacecraft Center has established a solar proton forecasting network (SPAN) consisting of three radio and optical observatories to support their prediction analyses (Ref. 12). The observatories are located in Carnarvon, Australia, the Canary Islands, and Houston, Texas. Most of the RF data used in the forecasting system established for the *Mariner V* mission were provided by these observatories via SDFC.

B. Description of SDFC Facilities and Services

Several types of forecasts of the probability of occurrence of proton events are provided by SDFC. These forecasts are issued for periods of 1, 2, 3, 7, and 28 days. The 28-day forecasts are based on location of active regions on the sun. The shorter-range forecasts are based on a number of parameters which are cross-correlated with solar activity. The 28- and 7-day forecasts are provided in routine weekly TWX's. The 1-, 2-, and 3-day forecasts are provided in TWX's twice daily.

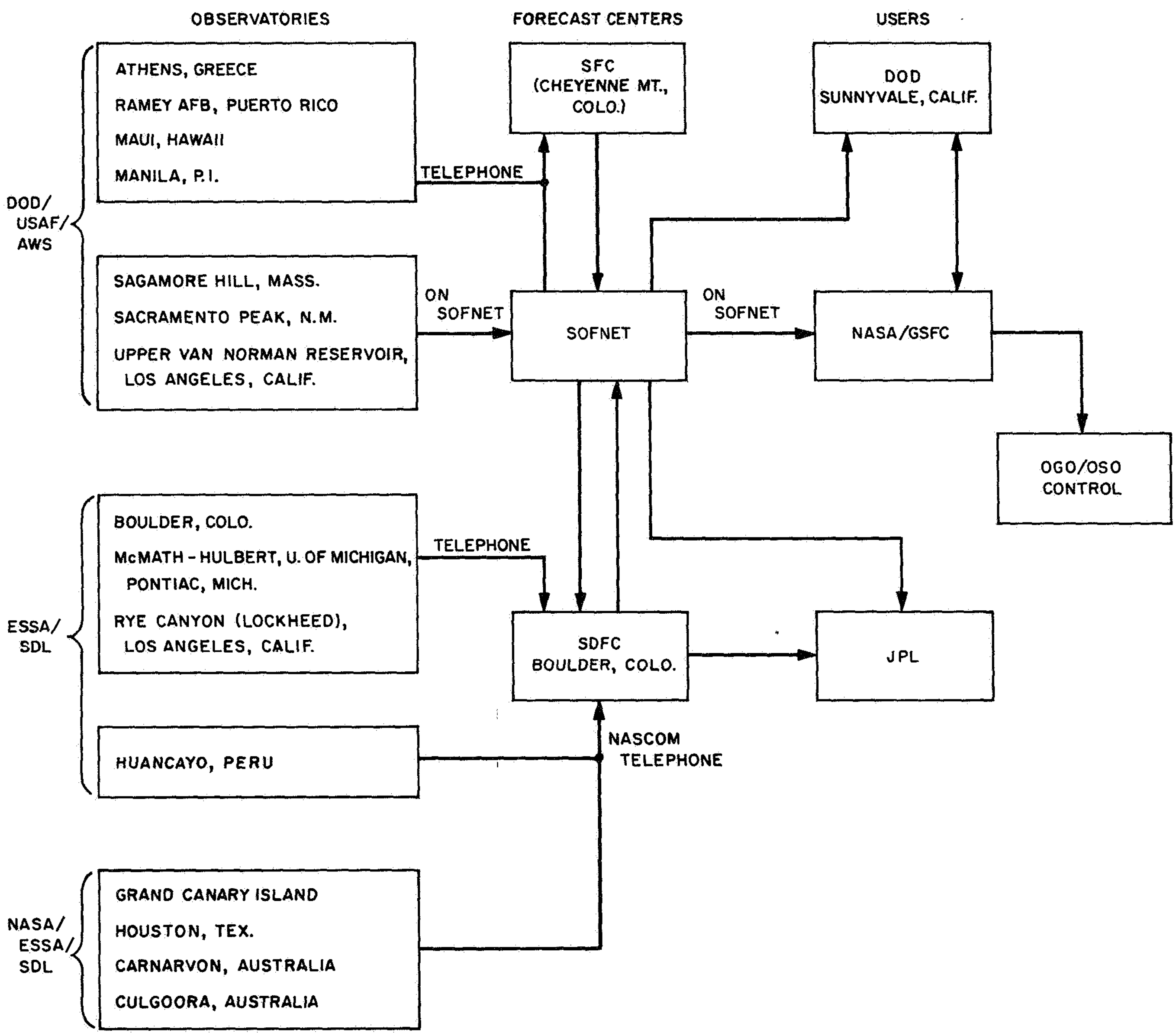

Fig. 19. Solar flare warning system

Table 16. Network of solar observatories supplying information to Space Disturbance Forecast Center[a]

Observatory location	Supported by DOD	Supported by NASA/ESSA	Radio	Optical	Observatory patrol times (±1 h), UT	Real-time patrol site	Reports of flares of class 2 or greater		Routine reports	
							Communications system	Time to SOFNET, min	Communications system	Time to SOFNET, min
Athens, Greece	✓			✓	04–16	✓	Mil Tel to Ent (SOFNET)	5	Mil WXTT to TIK (SOFNET)	30
Capri, Italy		✓		✓	05–17		Com Tel to Naples Mil Tel to Ent (SOFNET)	25	Mil TWX to Belvoir (SOFNET)	1-day report
Wendlestein (Germany), Nera (Holland), Meudon (France)				✓	06–18		Com Tel to Frankfurt Mil Tel to Ent (SOFNET)	20	Mil TWX to Belvoir (SOFNET)	1-day report
Grand Canary Island		✓	✓	✓	07–19	✓	NASA Tel to Boulder	2	NASA TWX to GSFC (SOFNET)	30
Ramey AFB, P.R.	✓			✓	10–22	✓	Mil Tel to Ent (SOFNET)	5	Mil WXTT to TIK (SOFNET)	15
Sagamore Hill, Mass.	✓		✓		11–23	✓	SOFNET	0	SOFNET	5
NRL, Washington, D.C.				✓	11–23		Com Tel to Belvoir (SOFNET)	3	Com Tel to Belvoir (SOFNET)	Beginning of day report
Huancayo, Peru		✓		✓	11–23	✓	Com Tel to Jicara ESSA Tel to Boulder (SOFNET)	5	NASA TWX to GSFC (SOFNET)	30
Ottawa, Canada			✓		12–24		Com Tel to Boulder (SOFNET)	3	Com Tel to Belvoir (SOFNET)	15
Pontiac, Mich. (McMath-Hulbert)		✓		✓	12–24	✓	Com Tel to Boulder (SOFNET)	3	Com Tel to Boulder (SOFNET)	15
Houston, Tex.		✓	✓	✓	12–24	✓	NASA Tel to Boulder (SOFNET)	3	NASA TWX to GSFC (SOFNET)	15
Boulder, Colo.		✓	✓	✓	13–01	✓	Com Tel to Boulder (SOFNET)	2	SOFNET	5
Sacramento Peak, N.M.	✓			✓	13–01	✓	SOFNET	0	SOFNET	5
Los Angeles, Calif. (Van Norman Reservoir)	✓		✓	✓	14–02	✓	SOFNET	0	SOFNET	5
Los Angeles, Calif. (Lockheed, Rye Canyon)		✓		✓	14–02	✓	Com Tel to Boulder (SOFNET)	3	Com Tel to Boulder (SOFNET)	30
Los Angeles, Calif. (Mt. Wilson)				✓	14–02		Com Tel to Boulder (SOFNET)	3	Com Tel to Van Norman (SOFNET)	30
Stanford, Calif.		✓	✓		14–02		Mil TWX to Ent (SOFNET)	15	Com Tel to Belvoir (SOFNET)	15
Maui, Hawaii	✓	✓		✓	16–04	✓	Mil Tel to Ent (SOFNET)	5	Mil WXTT to TIK (SOFNET)	30
Culgoora, Australia		✓	✓	✓	20–08	✓	Com Tel to Canberra NASA Tel to GSFC (SOFNET)	5	Com Tel to Canberra NASA TWX to GSFC (SOFNET)	30
Tokyo, Japan			✓		21–09		Com Tel to Fuchu, Japan Mil Tel to Ent (SOFNET)	15	Mil TWX to Belvoir (SOFNET)	60
Manila, P.I.	✓	✓	✓	✓	22–10	✓	Mil Tel to Ent (SOFNET)	10	Mil WXTT to TIK (SOFNET)	30
Carnarvon, Australia		✓	✓	✓	22–10	✓	NASA Tel to Boulder (SOFNET)	2	NASA TWX to GSFC (SOFNET)	30
Tehran, Iran	✓			✓	02–14	✓	Mil Tel to Ent (SOFNET)	5	Mil TT to TIK (SOFNET)	30

[a]Abbreviations and place names appearing herein are defined as follows:

- Belvoir — Ft. Belvoir, Va.
- Boulder — Boulder, Colo. (Space Disturbance Forecast Center)
- Com Tel — commercial telephone
- Ent — Ent AFB Colo.
- Mil Tel — military telephone
- SOFNET — Solar Observatories Forecast Network: Teletype loops connecting all U.S. solar observatories to the Space Disturbance Forecast Center at Boulder, Colo., the Astrogeophysical Forecast Facility at Ent AFB, Colo., Goddard Space Flight Center, Greenbelt, Md., Ft. Belvoir, Va., and Tinker AFB, Oklahoma City, Okla.
- TIK — Tinker AFB, Oklahoma City, Okla.
- WXTT — wireless teletype

The SDFC service also includes transmitting data received from observing stations to users. Under special arrangements, data transmitted to SDFC by a participating station are not generally interpreted, but SDFC will interpret information for its users upon request. In addition, SDFC provides data on other activity parameters, including the class of optical flares, plage area, brightness, sunspot area, magnetic complexity, and any proton data available to it from earth-based detectors, satellites, and probes.

C. Techniques and Criteria Used to Obtain Radio Burst Energy

1. Calculations of area of radio burst profile. The area under the curve of the radio burst flux-vs-time profile is computed by a numerical integration (Appendix B). The RF energy used in the prediction is shown in Fig. 20 as the area under the curve. The prediction techniques use the area remaining under the burst profile after the base line of the profile is raised by 10% of the peak value. This part of the burst profile was selected because the only areas available in the literature are the areas of the burst profile greater than the 10% difference. Studies of the radio burst profile indicated that use of this part of the area eliminated the results of postburst increase (Fig. 2) in the smaller bursts, where the postburst increase may contribute significantly to the burst profile area.[8]

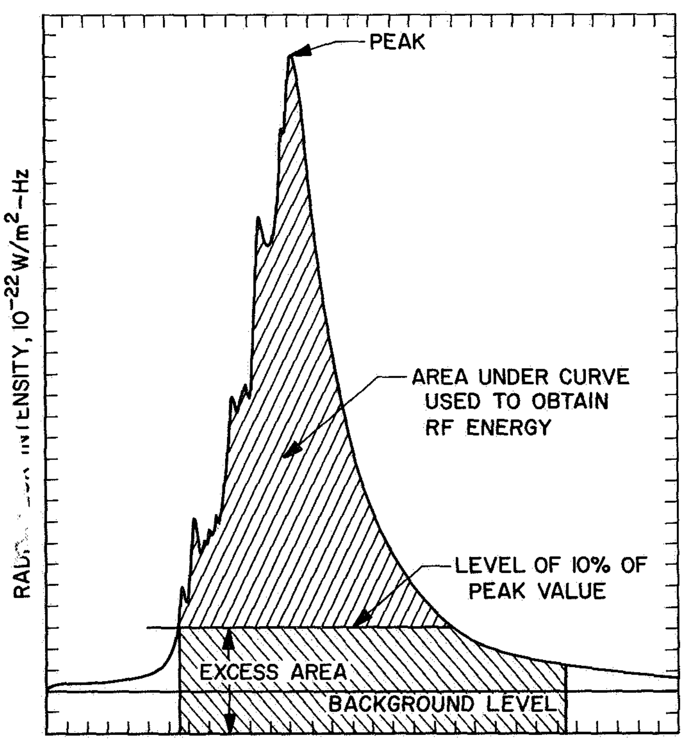

Fig. 20 A typical 2800-MHz radio burst profile showing the areas to be evaluated

2. Selection of data interval. Two considerations are important in determining the time interval for recording and transmitting. First, the burst profile data should provide an accurate determination of the proton flux; second, the time interval for transmitting the real-time data should minimize delay time prior to forecasting.

The time intervals were determined using four representative burst profiles from the last solar cycle and one from this cycle. Points were taken from the curves at 30-s intervals. The numerical procedure described in Appendix B was used to compute the burst profile area using data points separated by 30-s, 1-min, 2-min, 4-min, and 8-min intervals. Each of these burst profile areas was substituted into Eq. (1) to obtain corresponding proton fluxes. Then proton fluxes for each event were obtained by substituting burst profile areas, determined by planimeter, into Eq. (1). The planimeter-related proton fluxes were normalized to 1.0, and the corresponding proton fluxes determined numerically for each event were normalized using the planimeter-related fluxes. The results (Table 17) show that significant differences in computed fluxes may occur when the time interval on the radio event data is greater than 4 min.

Table 17. Comparison of time-integrated proton fluxes using the RF energy prediction method and RF energies computed using data points separated by different time intervals[a]

Events	Normalized time-integrated flux — Time intervals on radio flux data: 30 s	1 min	2 min	4 min	8 min
11/12/60	.904	.916	.897	.887	.775
11/20/60	.981	.966	1.036	.918	.954
7/17/61	.957	.960	.975	.898	1.240
7/20/61	.978	.985	.969	.778	2.040
7/7/66	1.099	1.111	1.158	.893	1.777

[a]Proton fluxes computed using RF energies determined by use of a planimeter on the radio burst profile equal 1.0

Partial areas were computed, using data points taken for specific intervals of time, to determine whether a reliable estimate of the total area could be made before

[8]M. D. Lopez (see footnote 3).

all burst profile data points were transmitted. If after some time into the burst a reliable estimate could be made, then data should be transmitted at least at this time interval. The method of partial areas did not indicate any feasible way of making a prediction of area before burst termination. Therefore, a prediction of proton flux before the end of burst requires a different procedure. Correlation of flux with the radio peak flux may provide a procedure, since an increase in radio flux beyond certain limits indicates a large event. For large proton events, the threshold radio peak flux value may be exceeded 2 to 4 min after the start of a burst. Data transmitted at 4-min intervals are adequate for this purpose.

3. ***Selection of RF flux level criteria.*** Radio burst data from SDFC were received for use in the proton flux prediction techniques when the radio flux increased 500 flux units over background. An attempt was made to exclude as many false alarms as possible and still not miss any major events. One can see by looking at the peak flux values in Table 3 that only one proton event in the last cycle with integrated flux greater than 5×10^7 protons/cm^2 would have been missed if radio events whose flux never increased beyond 500 flux units above background were ignored.

D. Checkout of Operational Network

On October 30 and 31, 1967, simulated data on solar activity including proton events were provided by SDFC. The simulation was primarily performed for the Apollo Project at MSC but with JPL invited to participate. Proton data from riometer stations, however, were sent from Anchorage directly to Houston via teletype lines and were not available to JPL. JPL received information on general solar activity, radio emission data, and some *Pioneer* proton data.

The simulation of solar activity consisted of five solar events. Sufficient radio data on two events were provided for use in the regression equations. In the one event, the peak radio flux (1520 flux units) at 2695 MHz was provided 20 min after the event was to have occurred. RF burst data at 2695 MHz can be used in place of 2800-MHz burst data. The regression equation for peak radio flux vs integrated proton flux was used to estimate the expected integrated proton flux for particles of energies greater than 30 MeV. The value obtained was 1.80×10^7 protons/cm^2 based on a peak flux of 1520 flux units, with a 95% confidence interval of 5.0×10^5 to 6.0×10^8 protons/cm^2. No proton flux data were reported on this event. In another event, radio data at 2695 MHz from the Sagamore Hill Observatory (Massachusetts) were transmitted, starting 30 min after initial solar activity was reported (including a Sb flare). The burst had started 6 min after the initial report. The radio burst lasted 48 min, and the last data were sent 15 min after the termination of the burst. The data were transmitted in sufficient detail to be used in the regression equation derived for the radio burst energy vs integrated proton flux. A value for the integrated proton flux above 30 MeV of 3.5×10^6 protons/cm^2 with a 95% confidence interval of 7.0×10^5 to 2.0×10^7 protons/cm^2 was obtained based on a computed burst energy of 52 (10^{-18} J/m^2-Hz). Again, no proton flux data were reported. The radio event coincided with a 3b white light flare.

In the other events (and in the two mentioned above) the general solar activity data reported were sufficient to indicate impending solar activity, but no quantitative predictions of a proton event could be made. Data and information reported included:

(1) Plage brightness and area.

(2) Sunspot area.

(3) Flare area and position with respect to associated sunspots.

(4) Ionospheric effects (due to electromagnetic radiation accompanying the optical part of the flare).

In one of the events, 3 h after the active region was first reported, *Pioneer VI* particle data were reported. Data from *Pioneer VI* were again reported 1 h later and from *Pioneer VII* 3½ h later. The following data were reported:

(1) Solar wind velocity.

(2) Cosmic ray data: counts per min over four energy ranges and quiescent values (the latter for *Pioneer VI* only).

(3) Interplanetary magnetic field information.

(4) Qualitative information on the H^+ density and temperature.

The *Pioneer* data would be especially useful for one concerned with a spacecraft in interplanetary space; and an estimate of the solar cosmic ray flux in space could have been made (at least with *Pioneer VI* data). The additional information would be useful if a particle propagation model was incorporated into the proton event forecasting techniques.

The results of the simulation were evaluated to deter mine the type of information gained about the operation of the forecast system and the type of information on solar activity available for use in the prediction techniques.

First, on the operation of the alert system, the simulated data were devised for the exercise on the basis of past experience. Moreover, time delays in transmitting real-time data were made to conform to those expected from past experience. The delay in receiving the radio data from Sagamore Hill was about 15 to 20 min after the time of observation. Information such as this is useful in estimating the effectiveness of the system; and no difficulties are anticipated on the basis of the time delays indicated in the simulation. The experience obtained in the simulation indicates that a direct link between cognizant personnel and SDFC would facilitate reception and comprehension of information.

Solar cosmic ray data made available from the *Pioneer* probes indicate that data may be available to confirm proton flux estimates made after a radio burst. Moreover, the data might be used in forecasting techniques which account for proton propagation in space. The inclusion of such data in forecasting proton events is necessary because predictions based on measurements of solar parameters from earth are used to forecast proton fluxes in interplanetary space. Finally, it might be useful to receive real-time proton data based on riometer data to determine the type of data being transmitted and the associated time delays in obtaining the proton data.

E. Recommended Procedures for Forecasting Solar Proton Events

The forecast procedure developed to evaluate solar activity and to predict proton events on a real-time basis in preparation for the *Mariner* 1967 Venus encounter is shown in the flow chart given in Fig. 21. A time span of 28 days is covered from the initial forecast of possible solar activity until the final period, when possible proton activity is imminent. The procedures are listed step-wise, each step being dependent on the information obtained in the prior step. The sequence of events is shown in Table 18. The times indicated are based on past experience and can fluctuate for specific cases.

The forecast procedures are described below as applied to any interplanetary mission. Active periods may be forecast from the 28- and 7-day solar activity predictions. The 28-day solar activity predictions are repeated weekly

Table 18. Sequence of events in the time span from a 28-day prediction to the occurrence of a solar proton event

Time	Event
−28 days	−28-day SDFC prediction on solar activity
−7 days	−7-day SDFC prediction on solar activity
−3 days	−3-day SDFC prediction on flares and proton events
−2 days	−2-day SDFC prediction on flares and proton events
−1 day	−1-day SDFC prediction on flares and proton events
−1 day–0	SDFC special arrangement notification of unusual or imminent solar activity
0	Peak optical intensity of flare
0–15 min	SDFC special arrangement notification of solar flare activity
0–1 h	Data on RF emission from SDFC, also solar activity parameters such as associated plage area, brightness, sunspot area, and flare intensity
1–2 h	RF emission data and any riometer data (proton-induced) from SDFC
2–24 h	Proton data (riometer data, onset times, etc.) from SDFC
24–100 h	Postevent data from SDFC

and thus can be updated. The 28- and 7-day forecasts are simply used to establish periods of time when solar activity is expected. No actual predictions of proton events are made based on these forecasts.

The 1-, 2-, and 3-day forecasts lead to alerts that define periods of possible proton activity. In addition, the 1-, 2-, and 3-day forecasts may lead to definite action by cognizant personnel. There are three levels of action which can be taken. In each case cognizant project personnel are advised of the pending activity. In the case of a forecast of high solar activity (with the expectation of a proton event), cognizant personnel are put on a 24-h alert. During this time, contact is maintained with SDFC via telephone to evaluate the solar activity. The forecast of high solar activity and possible proton events is based on changes in size and brightness of the active region, the past history of the region, and the magnetic complexity of the associated sunspots. Moderate activity with low expectation of proton events would be another possible forecast. This prediction would involve the existence of active regions of size, brightness, and magnetic complexity different from those regions producing proton events. In this case, through special arrangement with SDFC, cognizant personnel are informed of any changes in the active regions which might produce a proton event. If the activity increases significantly, the status of the alert would be the same as that employed during the high solar activity. For low activity, where the active regions

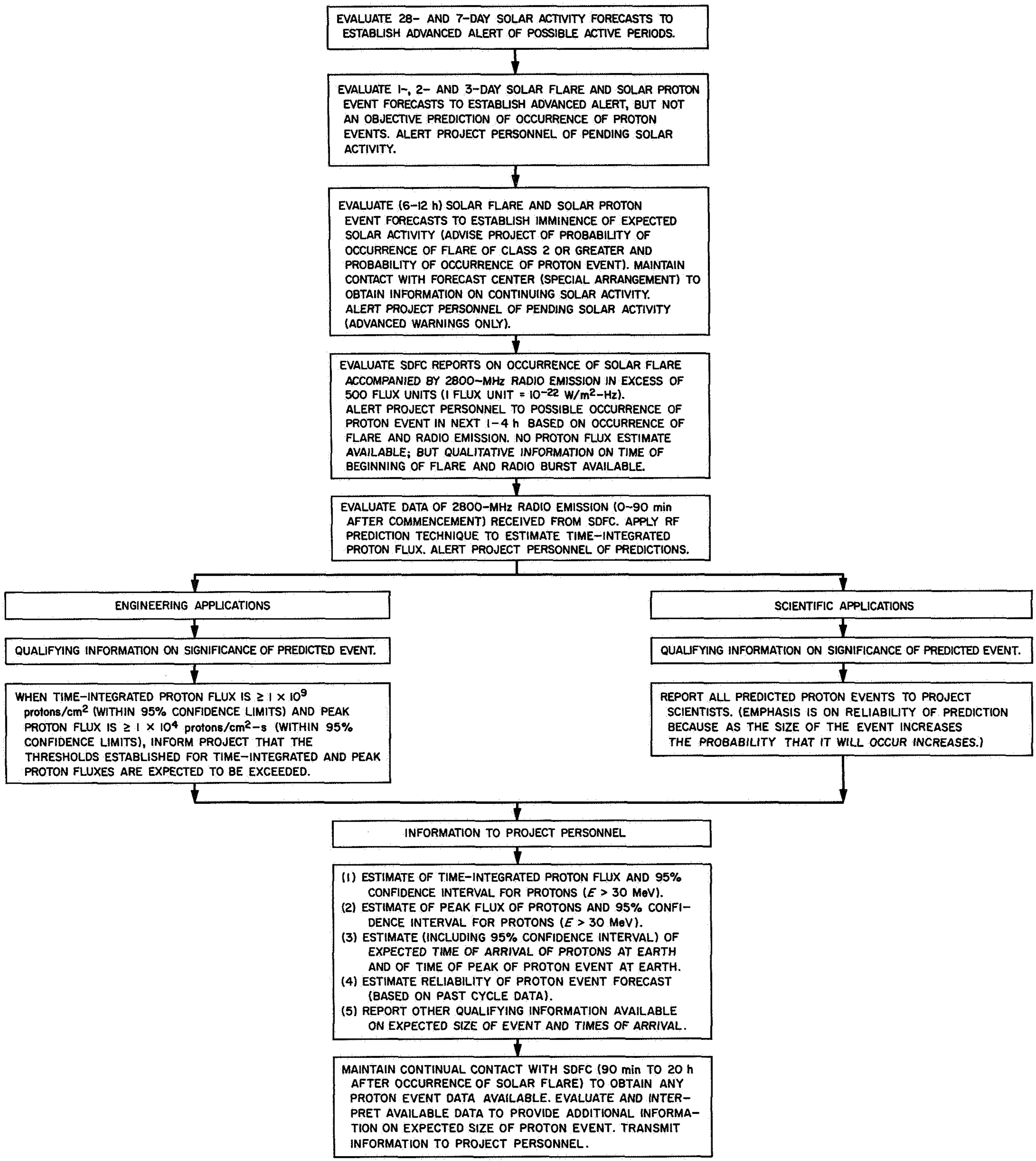

Fig. 21. Operational procedure for forecasting solar proton events used for *Mariner V* Venus encounter, October 19, 1967

are very small or declining rapidly and no activity is expected, cognizant personnel will use TWX to follow the situation. However, the special arrangement with SDFC will be used in the event of changes in the situation.

The next level in the forecast procedure is the actual occurrence of a radio event with an increase in the radio flux of 500 units above the background level. Normally, radio events occur at times of predicted high solar activity and cognizant personnel will be available to receive the radio data in real-time. Problems may arise causing a delay in the transmission of radio data. However, as soon as the commencement of the radio burst is reported, the following information may be reported to the appropriate mission operations support personnel:

(1) Confirmation of the radio burst and the expected proton event, with supporting qualitative information as to the expected size of the proton event and other characteristics of solar activity.

(2) Time of beginning of the radio burst.

(3) Related statistical information on RF burst and proton event delay times (Table 4).

When additional RF data reported are sufficient to make the estimates of the time-integrated proton flux, the following information may be reported to cognizant project personnel.

(1) Estimate of the time-integrated proton flux and the associated 95% confidence limits for protons of energies greater than 30 MeV.

(2) Estimate of the peak proton flux and the associated 95% confidence limits for protons of energies greater than 30 MeV.

(3) Estimate as to whether the time-integrated proton flux within the 95% confidence limits exceeds 1×10^9 protons/cm^2 and/or the peak flux within the 95% confidence limits exceeds 1×10^4 protons/cm^2-s.

(4) The probability of false alarms occurring for the predicted time-integrated proton flux.

(5) Estimate as to whether the event is expected to affect the operation of spacecraft subsystems.

(6) Time of termination of the radio event.

When the data reported are not sufficient to make a prediction of the proton time-integrated flux, this fact is reported to cognizant project personnel with qualifying information. Any additional information or data (e.g., spacecraft or ground-based measurements) received from SDFC on actual proton fluxes will be evaluated and included in the forecast to cognizant project personnel.

F. Solar Forecast System and Forecast Procedures Used During *Mariner V* Mission

The forecast procedures established for the *Mariner V* encounter sequence were followed. But because the sun was very inactive during the several months before and during encounter, only the network services consisting of daily routine TWX's and reports of very-low-energy particle events were used. One solar proton event was forecast and was evaluated as follows:

Data were transmitted for a small event which occurred from 2359 to 0050 UT on August 18–19, 1967, after the radio flux exceeded the initial criteria of 500 flux units. At 0105 UT (August 19) the JPL answering service received notification of the radio event in the form of a peak flux and preburst level. At 0236 UT the JPL answering service received preburst levels and 5 data points spaced about 10 min apart. The burst was small and indicated an energy of about 50–100 (10^{-18} J/m^2-Hz), giving a time-integrated flux estimate 7.5×10^6 protons/cm^2 for 75 (10^{-18} J/m^2-Hz). The proton flux estimate and 95% confidence interval of 1.5×10^6 to 4×10^7 protons/cm^2 was reported to the *Mariner V* cognizant project personnel as information only to complete the alert cycle because the threshold limit established on time-integrated proton flux was not exceeded. No proton event was reported as of August 21, 1967, 2235 UT.

VI. Conclusions

The forecast system and operational procedures based on statistical analyses of past solar cycle data allow timely and reasonably reliable predictions of proton events and their sizes on a real-time basis. The solar forecast system was established to alert both engineering and scientific personnel in mission operations of pending solar activity. The RF prediction techniques provide estimates of the time-integrated proton flux, and when the scientific or engineering requirements are met, the forecasts are reported to the project for use in decisions concerning the mode of operation of the spacecraft and priorities for spacecraft tracking and scientific data collection.

SDFC and the network of solar observatories provided the information and data necessary to make the solar proton event forecasts. The time delay between recording the radio burst at the observatory and reception of the information at JPL is about 15 to 20 min. The prediction techniques are readily applied during the burst and after all the data are received. A delay of only a few minutes occurs in transmitting the subsequent forecast and recommendations to the project. After the occurrence of a radio event the prediction techniques developed provide forecasts of time-integrated proton fluxes from 15 min to 3.5 h before the arrival of protons at earth and at least 3 h before the peak proton flux reaches earth.

The operational procedures followed during the period of Venus encounter (October 19, 1967) were applied, but since the sun was quite inactive only minimum alert conditions were imposed. The procedures consisted of monitoring the SDFC daily TWX's and making a report to the project of the inactivity of the sun as required.

Of the single-parameter correlations made, the highest correlation coefficient was obtained by correlating the 2800-MHz burst energy with time-integrated proton flux. The correlation of the 2800-MHz peak radio flux with time-integrated proton flux also proved useful as a preliminary predictor. It is more timely, but it is not as reliable as the radio energy as a predictor. More complete analyses were performed using single-parameter correlations than were performed using multiple-parameter correlations because the latter did not significantly improve the results. However, as more data become available, a multiple correlation and regression study may produce a more timely and reliable predictor.

The reliability analysis of the prediction techniques was limited by lack of data from the last cycle. Facilities for acquiring the data, however, have been expanded by NASA owing to the Apollo effort, and as solar radio and proton events occur in the present cycle it may be possible to obtain better resolution in the false alarm and miss frequency predictions.

Forecasts of the occurrence of proton events can be verified and the forecasts of their magnitude may be continually refined by using available real-time proton data obtained from satellite sensors, neutron monitors, and directly measured data (mainly riometer absorption) taken during the early phase of the event (Ref. 15). Real-time data from the ground-based system including neutron monitors and riometer stations may be available in the future through SDFC, starting on a trial basis in early 1968. A more rigorous study of the propagation of protons in space is required in order to make accurate predictions of the environment at the position of the spacecraft in interplanetary space.

VII. Recommendations

The solar forecast system developed for the *Mariner V* Mission should be implemented with appropriate modifications for interplanetary missions in the time span 1968–1971. The recommended modifications are described below:

(1) A new data compilation should be made and additional statistical analyses should be performed to improve the existing correlation and false alarm probabilities.

(2) Statistical analyses of radio burst data and correlations of radio burst data with proton flux data should be performed at 2800 MHz and other frequencies. These analyses should include both single frequencies and combinations of frequencies. Also, other solar parameters should be statistically studied.

(3) Forecast reliability analyses should be performed to include all known factors which influence reliability.

(4) Techniques using available real-time proton data in combination with the RF techniques to predict both time-integrated and peak proton fluxes should be studied.

(5) The propagation of particles in interplanetary space should be analyzed, with consideration given to the location of the flare on the sun's disk and transport of particles to the spacecraft.

(6) Facilities for receiving and analyzing data from SDFC should be automated to ensure a more effective system.

Appendix A
Flare Classification

Flare class or importance is assigned in accordance with established scales. In the past, classification was based on the corrected area of the flare at the time of maximum brightness. Currently, a dual scale incorporating both area and intensity is used. The two systems are contrasted in Table A-1.

Table A-1. Flare class or importance

Corrected area, solar hemisphere $\times 10^{-6}$	Old system	New system[b]		
< 100	1−	Sf	Sn	Sb
100–250	1, 1+[a]	1f	1n	1b
250–600	2, 2+[a]	2f	2n	2b
600–1200	3	3f	3n	3b
> 1200	3+	4f	4n	4b

[a]Plus sign indicates intensity, line width, or duration greater than normal.
[b]f = faint; n = normal; b = brilliant.

Appendix B

Calculation of Area of Radio Burst Profile

The numerical integration to obtain RF burst energy is performed by taking five points on the curve (Fig. B-1), the last point in each calculation being the same as the first point in the next calculation.

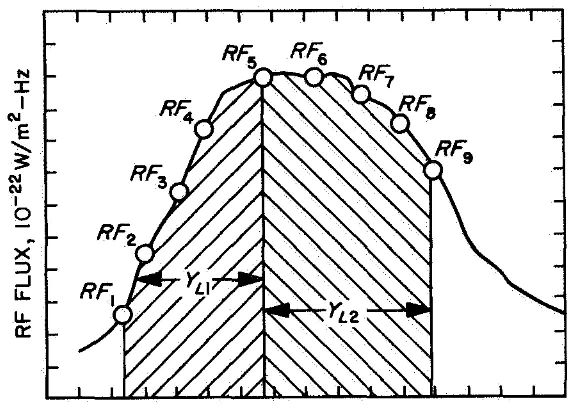

Fig. B-1. Partial areas under radio burst profile used in numerical integration technique to evaluate RF energy

The following quantities are defined:

$$H = 4.0 \times \text{(time interval between values of RF flux in seconds)}$$

$$RF_i = i\text{th value of radio flux in units of } 10^{-22}\text{W/m}^2\text{-Hz}$$

$$X_1 = 7.0 \times (H) \times (RF_1) \times 10^{-4}$$

$$X_2 = 32.0 \times (H) \times (RF_2) \times 10^{-4}$$

$$X_3 = 12.0 \times (H) \times (RF_3) \times 10^{-4}$$

$$X_4 = 32.0 \times (H) \times (RF_4) \times 10^{-4}$$

$$X_5 = 7.0 \times (H) \times (RF_5) \times 10^{-4}$$

$$Y_{L1} = (X_1 + X_2 + X_3 + X_4 + X_5)/90$$

(Y_{L1} represents the partial area under the curve in units of 10^{-18} J/m^2-Hz)

The next partial area is found in the same manner, and the calculation is repeated until the entire area under the curve is covered.

The area of the curve of interest is chosen in the following way: A flux value which is 10% of the peak value of the curve is selected as indicated on Fig. 20. The RF_1 value is selected at the intersection of the 10% line and the curve. Subsequent RF values are then selected at an equal time interval along the curve for use in the numerical integration technique. The area computed will include an excess area as shown in Fig. 20. This area must be subtracted from the numerically computed area to obtain the area above the 10% line.

Glossary

Flare	a sudden increase in solar radiation which may fall in the X-ray, UV, or radio parts of the spectrum, but generally is in the visible part.
Flare class or importance	determined by flare area and intensity (see Appendix A).
OGO	Orbiting Geophysical Observatory.
OSO	Orbiting Solar Observatory.
Peak	peak flux of solar radio event, 10^{-22} W/m^2-Hz.
PF	solar proton event time-integrated flux for energies greater than 30 MeV.
Plage	a bright area in the chromosphere of the sun.
Plage area	area of sun's disk, covered by a plage, solar disk $\times 10^{-6}$.
Plage brightness	optical intensity of brightest part of plage, on a scale of 1 to 5.
RF	solar radio frequency burst emission at the time of a flare.
RFE	solar radio frequency burst emission energy, 10^{-18} J/m^2-Hz
SDFC	Space Disturbance Forecast Center.
SOFNET	Solar Observatories' Forecast Network.
Solar proton event	solar proton emission at the time (within several hours) and from the region of a flare.
Solar radio event	solar radio emission at the time (within several minutes) and from the region of a flare.
Sunspot	small region in the photosphere of the sun which is darker than the surrounding area.
Sunspot area	area of a sunspot, solar disk $\times 10^{-6}$. (When it is correlated with a solar proton event the area represented is that of the sunspots associated with the active region producing the proton event.)
S_x	estimated standard deviation of radio burst energy of x actual events from the average event energy.
S_{yx}	estimated standard deviation of predicted flux of y proton event using x radio event from actual flux of proton event.
Type IVμ radio emission	radio emission in the microwave region (from the solar atmosphere) at the time of a solar flare believed to be electron-induced synchrotron radiation.
X	$\log_{10}$ of radio energies at which confidence limits were computed.
$\bar{X}$	$\log_{10}$ of average radio energy.
X_i	$\log_{10}$ of the radio energies of selected events.

Glossary (contd)

Y_i' $\log_{10}$ of predicted estimate of integrated proton flux from a regression equation relating proton flux and radio burst energy.

Y_i $\log_{10}$ of observed proton flux of the selected events.

References

1. Anspaugh, B. E., *High Energy Proton Testing of Mariner IV Components*, Technical Memorandum 33-314, Jet Propulsion Laboratory, Pasadena, Calif., Jan. 1, 1967.
2. Smith, H. J., and Smith, E. V. P., *Solar Flares*, The MacMillan Co., New York, 1963.
3. Webber, W. R., *Sunspot Number and Solar Cosmic Ray Predictions for Cycle 20 (1965–1975) with Preliminary Estimates for Cycle 21*, Report D2-113522-1, The Boeing Co., Seattle, Wash., 1967.
4. Yule, G. U., "On a Method of Investigating Periodicities in Disturbed Series, with Special Reference to Wolfer's Sunspot Numbers," *Phil. Trans.*, Vol. 226, Royal Society of London, 1926.
5. Wild, J. P., "The Radio Emission from Solar Flares," *J. Phys. Soc. Japan*, Vol. 17, Supplement A-11, pp. 249–258, 1962; International Conference on Cosmic Rays and the Earth Storms, Sept. 1961.
6. Fletcher, J. D., "Solar Radio Emission as a Criterion for Solar Proton Event Warning," *AIAA J.*, Vol. 2, p. 2193, 1964.
7. Kundu, M. R., *Solar Radio Astronomy*, Interscience Publishers, New York, 1965.
8. Maxwell, A., Defouw, R. J., and Cummings, P., "Radio Evidence for Solar Corpuscular Emission," *Planet. Space Sci.*, Vol. 12, pp. 435–449, 1964.
9. Takakura, T., and Ono, M., "Yearly Variation in Activities of Outbursts of Microwaves and Flares During a Solar Cycle with Special Reference to Unusual Cosmic Ray Increases," *J. Phys. Soc. Japan*, Vol. 17, Supplement A-11, pp. 207–210, 1962, International Conference on Cosmic Rays and the Earth Storms, Sept. 1961.
10. "Estimates of Proton Fluxes Expected In the Solar Flare Radiation Environment During Mariner Mars 1969 Missions," in *The Planetary-Interplanetary Program*, Space Programs Summary 37-41, Vol. II, pp. 32–39. Jet Propulsion Laboratory, Pasadena, Calif., Sept. 30, 1966 (Confidential).
11. Webber, W. R., *An Evaluation of the Radiation Hazard Due to Solar Particle Events*, Report D2-90469, The Boeing Co., Seattle, Wash., 1963.
12. Higgins, P. W., *Operational Procedures for Apollo Dose Radiation*, NASA SP-71, Second Symposium on Protection Against Radiations in Space, 12–14 October 1964, pp. 151–156.

References (contd)

13. *Solar Proton Manual*, Edited by F. B. McDonald, NASA TR R-169, Washington, Dec. 1963.

14. Dixon, W. J., and Massey, F. J., Jr., *Introduction to Statistical Analysis*, McGraw-Hill, New York, 1957.

15. Webber, W. R., *An Evaluation of Solar Cosmic Ray Events During Solar Minimum*, Report D2-84274-1, The Boeing Co., Seattle, Wash., 1966.